



Mathias Andreas Hobisch, BSc

Energy Storage Media based on Fines

MASTERARBEIT

zur Erlangung des akademischen Grades

Diplom-Ingenieur

Masterstudium Technische Chemie

eingereicht an der

Technischen Universität Graz

Betreuer

Mag. Dr., Stefan Spirk

Institut für Chemische Technologie von Materialien

Graz, November 2016

EIDESSTATTLICHE ERKLÄRUNG

Ich erkläre an Eides statt, dass ich die vorliegende Arbeit selbstständig verfasst, andere als die angegebenen Quellen/Hilfsmittel nicht benutzt, und die den benutzten Quellen wörtlich und inhaltlich entnommenen Stellen als solche kenntlich gemacht habe. Das in TUGRAZonline hochgeladene Textdokument ist mit der vorliegenden Masterarbeit identisch.

AFFIDAVIT

I declare that I have authored this thesis independently, that I have not used other than the declared sources/resources, and that I have explicitly indicated all material which has been quoted either literally or by content from the sources used. The text document uploaded to TUGRAZonline is identical to the present master's thesis.

Datum / Date

Unterschrift / Signature

Abstract

The starting material for paper-based products is wood. Since the market is steadily increasing, research is particularly interested on this branch of industry. As always, a special interest lies on the process optimization and decrease of the price for production while keeping high quality standards. A special interest for industry is the utilization of side stream products. In the recent years, research concentrated on lignin but nowadays a second very interesting side stream has been separated successfully, namely fines. Since the impairment of fines on paper has for years been known, investigations concentrated on the upscaling of the filtration plant. Fines are classified in mechanical and chemical fines, which can be further subdivided into primary and secondary fines. It is of utmost importance to distinguish between them, because properties differ.

A pilot plant enables the separation of fines up to kilogram, which entails research on applications based on fines. Size distribution is of particular interest, high surface areas and dense packing accompany the highly hierarchical order. Properties based on the size awakened the interest for filters and energy storage media, both applications prefer smaller particle and pore size. We concentrated on supercapacitors, which are energy storage media. Main advantages to batteries are high cycle life and specific power. The small particle size increases electrode space, which improves the adsorption of ions. Furthermore, the electrode material is doped with heteroatoms, the difference in electronegativity improves the interactions between electrolyte and electrodes, resulting in higher capacities. Followed by BET measurements to estimate the surface area and compare different activation methods without assembling supercapacitors. Electrode materials with the highest surface area were formed to electrodes and assembled inside a Swagelok®-cell. At the end, electrochemical measurements provide information about application specific parameters. Finally, an energy storage media has been produced out of an industrial side stream.

Kurzfassung

Holz ist das wichtigste Ausgangsmaterial für die Papierindustrie. Ein stetig wachsender Absatzmarkt macht Forschung besonders interessant. Ein besonderes Hauptaugenmerk liegt seit jeher auf der Optimierung des Prozesses. Dazu zählt, reproduzierbare Ergebnisse zu erhalten und gleichzeitig die Produktionskosten zu senken. Dies gelingt vor allem durch Wiederverwendung von Abfallprodukten. Seit Jahren wird an einer großtechnischen Lösung zur Nutzung von Lignin geforscht. Nun wurde ein weiteres Produkt für den zukunftssträchtigen Markt gefunden, so genannte Feinstoffe. Feinstoff ist in der Literatur schon länger bekannt, doch war es bisher unmöglich ihn großtechnisch abzutrennen. Der Einfluss von Feinstoffen auf Papierprodukte ist nicht zu unterschätzen. Aus diesem Grund wird nach alternativen Anwendungen gesucht. Feinstoffe können grundsätzlich in chemisch und mechanisch unterteilt werden. Beide unterscheiden sich stark in der Zusammensetzung und müssen getrennt betrachtet werden. Für chemische Feinstoffe gibt es eine weitere Unterteilung in primären, sekundären und tertiären Feinstoff. Während Primäre sich schlecht auf Bindungseigenschaften auswirken, stärken Sekundäre das Papier.

Durch eine Pilotanlage ist es erstmals möglich Feinstoff im Kilogramm Bereich zu gewinnen und dadurch tatsächliche Anwendungen zu prüfen. Eine sehr interessante Größenverteilung ergibt automatisch eine hierarchische Anordnung im Feinstoff. Dies erweckt vor allem das Interesse für Filter und Energiespeichermedien. Für beide Anwendungen ist die Porengröße entscheidend. Für Energiespeichermedien erhöht sich bei kleiner Porengröße die Oberfläche die für eine größere Adsorptionsfläche sorgt. Um die Oberfläche optimal nutzen zu können wird die Cellulose mit Heteroatomen gedopt. Durch Unterschiede der Elektronegativität können Heteroatome deutlich mehr Elektronen speichern. Zur Abschätzung der Oberfläche erfolgen BET Messungen, dadurch können unterschiedliche Aktivierungsmethoden und -temperaturen miteinander verglichen werden. Der elektrochemische Test erfolgt nach dem Einbau der Elektroden in eine Swagelok®-Zelle. Durch die Messung von Strom-Spannungskurven können nachweislich Aussagen über die Speicherfähigkeit des Materials getroffen werden. Dadurch kann aus einem Abfallprodukt der Papierindustrie ein Energiespeichermedium produziert werden.

Acknowledgements

At this point, I would like to thank my supervisor Dr. Stefan Spirk for his support during the master thesis, specifically for his experiences in the field of cellulose, his connections reaching far and wide outside of Austria and his helpful hand through scientific writing. Furthermore, I would like to thank Dr. Wolfgang Johann Fischer and Dr. Stefan Freunberger for their support and knowledge in fines and electrochemistry, both always offered a helpful hand during the thesis. Another very important person to acknowledge is the leader of the institute Prof. Dr. Franz Stelzer, who has supported me during the whole thesis. Special thanks also to Dr. Armin Zankel for the SEM measurements and his support in sample preparation.

Moreover, I want to thank the whole institute of ICTM, especially the laboratory staff for helping with various trials and measurements. I am also thankful to all Master- and PhD student who have helped me in the laboratory, and for being great colleagues and good friends.

Finally, a special thanks to my family for supporting me throughout all of my years of studying. I especially want to thank my mother and father for funding me, which has let me come that far in life.

Last but not least, I want to thank my friends, who have supported my whole life, and my study colleagues for always being there for me whenever needed.

Mathias Andreas Hobisch

Graz, November 11th 2016

List of abbreviations

AC	Activated Carbon
ACN	Acetonitrile
BET	Brunauer–Emmett–Teller
CV	Cyclic Voltammetry
DMF	Dimethylformamid
EDL	Electrochemical Double-Layer
EDLC	Electrochemical Double-Layer Capacitor
EDX	Energy-Dispersive X-ray Spectroscopy
GCPL	Galvanostatic Cycling with Potential Limitation
ICPMS	Inductive Coupled Plasma Mass Spectroscopy
IR	Infrared
LiFePO ₄	Lithium Ferrophosphate
PPy	Polypyrrole
PANi	Polyaniline
SEM	Scanning Electron Microscope
SC	Supercapacitor
TEABF ₄	Tetraethylammonium Tetrafluoroborate
TMP	Thermomechanical Pulp

Index

1. Theoretical background.....	1
1.1. Renewable resources	1
1.2. Wood	1
1.2.1. Paper manufacturing process	2
1.2.2. Fiber structure	4
1.2.3. Fines from wood.....	5
1.2.4. Properties	9
1.2.5. Composites with fines	11
2. Supercapacitors	12
2.1. Working principle	12
2.2. Electrode materials	16
2.3. Most common supercapacitors.....	18
2.3.1. Electrochemical Double Layer Capacitor.....	18
2.3.2. Pseudocapacitors	19
2.4. Components	22
2.4.1. Separator	22
2.4.2. Electrolytes	22
2.5. Supercapacitors and other energy storage possibilities	23
3. Electrochemical methods.....	24
3.1. Cyclic voltammetry	24
3.2. Galvanostatic cycling	26
3.3. Electrochemical Impedance Spectroscopy.....	27
3.4. Self-discharge and leak current.....	28
4. Analytical methods.....	30
4.1. Inductive Coupled Plasma Mass Spectroscopy (ICPMS)	30
4.2. Brunauer–Emmett–Teller (BET)	30
4.3. Scanning electron microscopy (SEM)	31
4.4. Energy-dispersive X-ray spectroscopy (EDX).....	32
4.5. Infrared Spectroscopy (IR).....	32
5. Materials and Methods	33
5.1. Preparation of chemical pulp	33
5.2. Activation process of fines	34
5.3. Composites with fines from wood	36
5.4. Fines from wood coated with conductive polymers	36

5.5.	Electrode preparation	37
5.6.	Cycling voltammetry and galvanostatic measurements	38
5.7.	Self-discharge and leak current.....	40
5.8.	Delithiation of LiFePO ₄	40
5.9.	Chemicals and materials.....	41
6.	Results and Discussion	42
6.1.	Process overview for activated carbons.....	42
6.2.	Elementary trace analysis.....	42
6.3.	Freeze drying of fines	43
6.4.	Activation processes.....	43
6.5.	Composites with fines from wood.	46
6.6.	SEM analysis	46
6.7.	Infrared Analysis (IR)	48
6.8.	Investigations of the purity of activated carbon	49
6.9.	Electrode manufacturing.....	50
6.10.	Electrochemical analysis.....	51
6.10.1.	EIS of EDLCs electrodes	52
6.10.2.	EIS of pseudocapacitor electrodes	52
6.10.3.	Supercapacitors with organic electrolytes	53
6.10.4.	Supercapacitors with aqueous electrolytes	59
6.10.5.	Comparing organic and aqueous electrolytes.....	62
7.	Conclusion and Outlook	64
7.1.	Future Outlook	65
8.	Attachments	66
8.1.	Figures	66
8.2.	Tables	68
8.3.	Bibliography.....	69

1. Theoretical background

1.1. Renewable resources

Ever since Johannes Gutenberg developed the printing process in 1400, paper production has been rising. In fact, production rate increased almost 100% in the last 20 years. About 400 million tons of paper were produced in 2013. Rising interest on production is one of the main reasons research is continued to optimize the process and enable progress. Developing novel conductive ink bases, filter models, electrode materials, and organic solar cells based on biological resources, are only a few of the major goals of research in the future. Side streams are particularly interesting because they are easily available and rather inexpensive. Cellulose (Fig. 1) is the most abundant biopolymer on earth and mostly applied for the above mentioned purposes. About 700 billion tons of cellulose are produced by lignocellulosic plants and microorganisms each year. This makes renewable research interesting compared to fossil materials like oil and coal. Furthermore, cellulose is fairly distributed all over the planet. The use of local renewable resources instead of fossil based ones can significantly reduce the amount of greenhouse emissions.

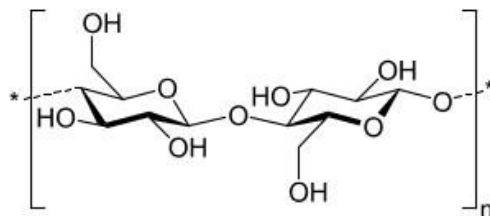


Figure 1 Basic molecular structure of unbranched cellulose, consisting of β -D-Glucose connected via β -1,4 glycosidic bond.

1.2. Wood

Wood is a natural, renewable and hierarchical organized material. Its easy accessibility makes it interesting for applications all over the world. It is a natural composite, which predominantly consists of cellulose, hemicellulose and lignin. All three components are embedded in a matrix, which provides resistance against mechanical impact (e.g. compression). Hemicelluloses and lignins contribute to stiffen the composite (Fig. 2). The cell wall consists of a middle lamella as well as a primary, secondary, and tertiary wall. Main tasks of cells are the storage and transport of water and nutrients. More than two-thirds of a tree are filled with air and tube

shaped fibers, which are connected to each other and enable the transport of water and nutrients.

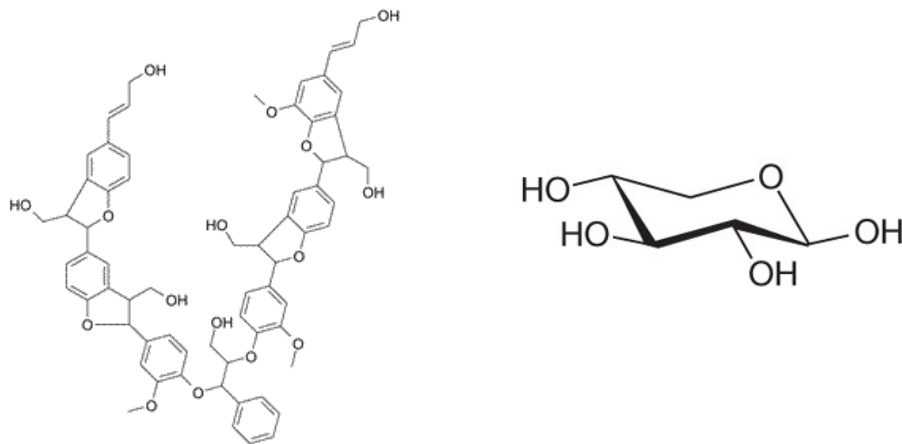


Figure 2 Simplified view on the molecular structure of lignin (left) and xylose (right), one of the most common pentose's in wood.

Two main types of trees grow on earth, namely hard and softwood. In the paper industry, mainly softwood is processed because longer fibers are preferred for papers. This approach has the advantage that a higher amount of bonds can be realized between the fibers. More bonds increase paper strength and flexibility. Hardwood is more packed than softwood. Fibers are much shorter causing higher density of fibers in wood. Further, differences in composition can be observed. Table 1 lists the distribution of all three main components, which are present in hard- and softwood. Predominantly, cellulose can be used for technical applications; therefore, trees containing high amounts of cellulose are preferred for technical processes.

Table 1 Comparing constituents of main wood species¹

Wood species	Cellulose [%]	Hemicellulose [%]	Lignin [%]
Hardwood	40-45	25-35	20-25
Softwood	40-45	25-30	25-35

1.2.1. Paper manufacturing process

The highly hierarchical matrix within trees, meant to protect and supply trees, makes it also hard to extract pure cellulose and harsh methods have to be applied to separate it from the other components. Different extraction methods have been applied in industry, but two main technologies are established in industry. The first technology comprises a mechanical treatment (e.g. refining, grinding etc.) for separation, which is highly energy demanding. This

process yields up to 97%² of cellulose. A further problem using this technology is abrasion of fibers. Abrasion breaks up to 40% of all fibers and as consequence the length of fibers is decreased. Therefore, the paper is denser due a more efficient packing of the fibers causing higher paper sheet prices. In the course of this mechanical process mainly secondary fines are produced. Comparing paper sheets of different processes, smooth surfaces and high bulks are also beneficial, but the bonding ability is lower and impurities are higher.² Additionally, mechanical pulps exhibit better brightness and higher light-scattering abilities than chemical pulp.

In contrast, chemical pulping disintegrates the wood matrix by cooking wood chips under harsh conditions. This procedure, called Kraft or Sulfite process, isolates the fibers without destroying or harming their integrity and fiber structure. However, a major disadvantage is the rather low cellulose extraction yield (ca. 35 - 65%) from the wood matrix, which depends on several factors such as the type of wood, and process related parameters like temperature. Both processes can pulp most types of wood, but certain woods are limited to one process. For example, eucalyptus can be only employed in chemical pulping. In this context, the influence of the type of pulping on the fiber properties should not be underestimated since breaking of bonds and abrasion are even visible in an optical microscope.

Chemical pulping also generates fines, but the final amount is about ten times smaller compared to mechanical treatments (Fig. 3).

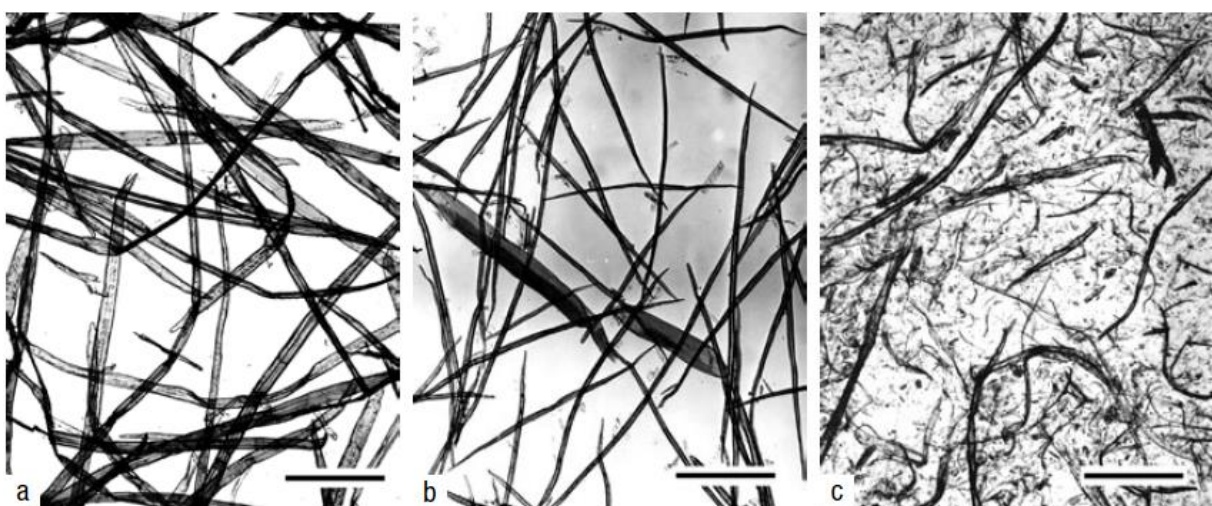


Figure 3 Unbeaten pulp of spruce (a) and birch (b) compared to thermomechanical pulp (c). The bar on the bottom is 400 μm .³

In more detail, the Kraft process removes lignin by cooking wooden pellets for a few hours in NaOH, sodium sulfide and sodium sulfate. It is mainly applied in the production of paper pulp and yields rather strong fibers. Remarkably high densities can be achieved by using Kraft fines to form a paper sheet, 1100 – 1200 kg/m³. This is very high compared to thermomechanical pulp (TMP) fines (450 kg/m³)⁴ and there is a direct influence on tensile index and light scattering as well. Although TMP fines reach the best light scattering, they usually feature rather poor tensile strengths.

Sulfite pulp processing is executed in a neutral or an acidic pH, depending on the salt (mostly sodium and calcium sulfites). Lignin reacts to form a ligninosulfonic acid, which can be easily separated from the mixture.

Mechanical pulp, also called “groundwood”, is produced by grinding wood against a rotating stone and further processed by passing a refiner. If additional heat treatment is involved, it is called thermomechanical pulping (TMP). When both technologies are applied, the hybrid product is called thermomechanical pulp (TMP).

Pulping, bleaching and refining have a large influence on final product properties affecting almost all of the physical properties. Tensile strength, light scattering, viscosity, and opacity are the most important to mention. All of these properties are determined by the fiber length distribution, which in turn is influenced by process abrasion. Mechanical pulping shreds up to 40% of all fibers, whereas chemical pulping minimizes milling to a maximum of 10%.³ Further information, like the hydration degree of the fine network can be obtained by viscosimetry.⁵

1.2.2. Fiber structure

The use of different fiber structures has a large impact on the properties of wet and dry paper. Since fines consist of grated fibers to major part, fiber structure is also important for investigations of fines. Figure 4 visualizes fiber structure in a rectangular form considering the most important layers.

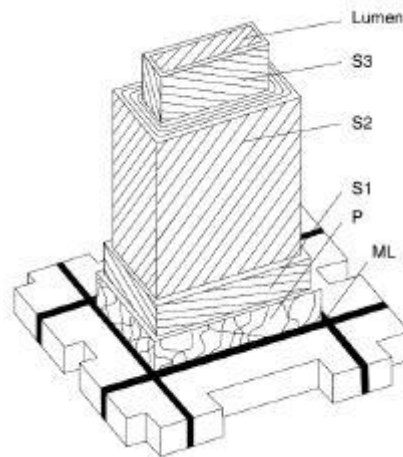


Figure 4 Fiber structure of a wooden fiber illustrating inner fiber layers³

In general, the wood cell wall consists of five different layers, primary wall (P), secondary walls (S1, S2 and S3) and the lumen. The outermost one is called primary wall (P), this layer is known to be feature a rather high degree of disorder. The three different middle layers, or secondary walls (S1, S2 and S3) are located between the P and the lumen. The thickness of the S1 layer range from 0.1 to 0.3 μm , it shows significant amounts of amorphous domains and is often destroyed during pulping. S2 is highly crystalline and its thickness covers a range from 1 to 5 μm . The crystalline cellulose domains are surrounded by mainly amorphous lignin. Since S2 is the thickest layer in the cell wall, it is dominating the mechanical properties. S3 (0.1 μm) is located at the interface to the lumen and it is mainly amorphous to protect the fiber from microorganisms. The lumen is the innermost and hollow part of the fiber. The thickness of fibers mainly depends on the type of tree, which is the reason for variations in the thickness of the different layers.

Besides the species, also environmental influences have a large impact on the fiber and cell wall dimensions.

1.2.3. Fines from wood

As mentioned previously, fines are a side stream of the paper manufacturing industry. Fines are shortened cellulose fibers already in wood, or generated by abrasion in the plant. They are produced throughout the whole process as mentioned above. About half of all fines originate from freshly harvested wood. The other half consists of reused materials, like old newspapers, wood fibers from sawmills and clothes. Therefore, it makes sense from an economic point of view to put efforts in the investigation of the properties of paper fines.

Higher forces in mechanical pulp processes increase the fines content compared to chemical pulp processes. Fibers stemming from trees reveal a fiber length of 0.8 - 7 mm with a thickness ranging from 14 to 65 μm . This equals an aspect between 50 and 100, depending on the type of tree. The length of fines is defined to be shorter than 0.2 mm. Contrary to fibers, fines have a length/thickness ratio of 1 to 5 which impacts the application areas. Consequently, properties change by minimizing the length/thickness ratio. First, surface area increases by decreasing the length of the fibers. The length of fines is located between fibers and nanofibrillated cellulose (NFC). Therefore, the distribution of the length is very important. Second, a distinction has to be made between different kind of fines, which is discussed later on. All fines stemming from chemical pulp have a bimodal size distribution (ca. 25 and 70-90 μm).⁶ As a result it can be distinguished between a finer and a coarser fraction, separation is achieved by ultracentrifugation. In that case, an individual analysis is possible.

TMP does not have these characteristics. On average, these fines are 25 μm long, with the same length/thickness ratio than fines from chemical pulp.

Figure 5 shows a microscopy image of the size distribution of fines. It can be easily clarified which kind of fines are used.

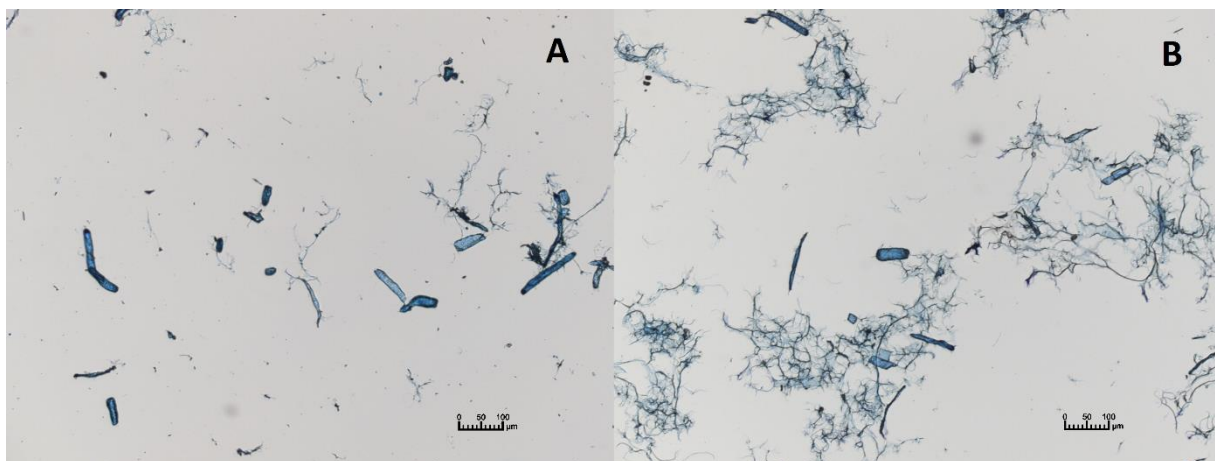


Figure 5 Image of an optical micrograph from primary (a) and secondary fines (b).

The finer fraction of fines is mainly due to abrasion, whereas coarse ones are shorter natural fibers. Beating leads to an increase of the fine fraction, whereas the coarse fraction is degraded. Mechanical abrasion causes the differences illustrated in Tab. 2 between mechanical primary and secondary fines. Interestingly, a different morphology can be observed comparing the results visualized by the bimodal graph.

In contrast to paper pulps, much higher amounts of lignin can be observed in fines independent of the used process. Unbleached Kraft paper pulp normally contains 5% of lignin. Chemical process pulps contain less lignin compared to mechanical ones and there are variations between primary and secondary fines. Although higher abrasion is the reason for building secondary fines, the lignin content of unbleached paper pulp is about 20% lower than for primary one. In a recent report, primary fines were reported to contain 23.4% of lignin.⁷

Fines also have an impact on sheet properties. Therefore, Tao Lin put his effort into comparing the influence of fines with fillers on the retention.⁸ The conclusion was that retention rate increases with higher fine dosage, while higher amount of fillers decrease it. Fines also change the brightness of a paper because of their size. By removing 4% of fines, brightness is increased by ca. 6% and also the brightness stability is improved.⁹ All morphological differences can be found in Tab. 2, below the differences are named and briefly described.

Table 2 Comparison between mechanical and chemical fines¹⁰

Type of fines	Origin	Main morphology	Content [%]
Mechanical	TMP	Fibrils, flakes, ray cells, lignin	10-40
Primary	Unbeaten chemical pulp	Ray cells, flakes from middle lamella	2-10
Secondary	Beaten chemical pulp	Fibrills peeled from fiber wall	2-10

Mechanical fines

The amount of lignin in mechanical fines is even larger. Mechanical forces separating the fibers are higher and grind lignin as well. The amount of fibers from secondary wall is much higher compared to chemical pulp fines, which leads to higher lignin contents. The predominant morphology of different fines is mentioned in Tab. 2.

Fibrils

Fibrils do not only contain fibril structures; they further consist of thin lamellas being part of fibrillary materials. They are rich in cellulose; therefore, they own a very high surface area.

Flakes

Flakes contain ray cells, wall fragments and thick lamellas. It is important to realize that cell wall contains lignin, thus it can be also detected in flakes

In Sundbergs work¹¹ the lignin content was reported to be higher in TMP fines compared to Kraft pulp fibers while cellulose content was reduced. Fines from flakes and ray cells on the other hand contain a lower amount of lignin and more cellulose. This indicates that fines originate from the primary (P) and secondary wall (S1), whereas a high amount of lignin indicates S2 as original source. Therefore the lignin/cellulose ratio allow for identifying the origin of the fines.

Primary fines:

Primary fines are rich in ray cells (Coarse fraction), fibrils and lamellas building the fine fraction. Depending on the ratio between coarse and fine fraction sheet properties vary. Again, smaller particles improve paper properties like density, which also increases bonding, whereas larger particles decrease it. Cole¹² measured the fines with a micrograph, confirming a ratio of 5 between length and diameter (Length is between 30 – 60 μm).

Secondary fines

Secondary fines are produced during beating of the pulp. Here, two different kind of fibrillation are observed, namely external and internal fibrillation. Fibrillation leads to an increase in surface area and therefore to increased fiber-fiber bondings improving sheet properties as well.⁴ An additional advantage of secondary fines is the faster dewatering compared to primary fines.

In a recent thesis⁶, the size distribution of used fines was discussed. Figure 6 illustrates the volumetric size distribution of primary and secondary fines of a primary unbleached Kraft pulp. Mechanical pulping minimizes the coarser fraction and further increase the fine one.

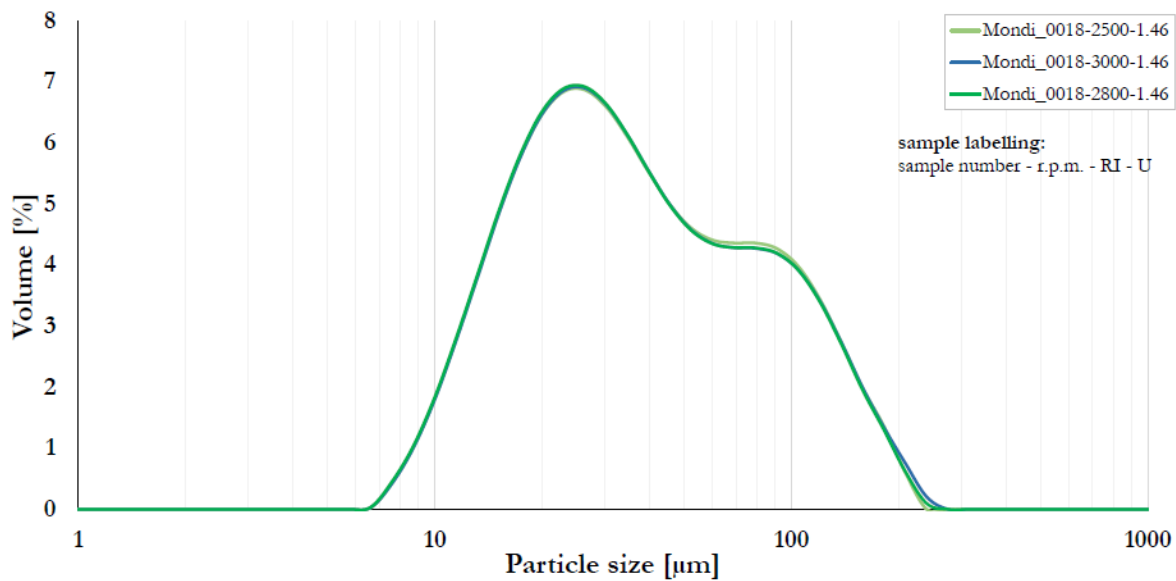


Figure 6 Primary fines from wood analyzed by the Malvern Mastersizer 2000, plotting a bimodal particle size distribution versus vol%.⁶

1.2.4. Properties

The evaluation of the influence of fines in typical paper products has been the subject of many studies in literature. The optimization of these products can be achieved by adjusting the amount of fines inside the sheets. By testing and characterizing different amount fines optimized proportions between fines and fibers can be applied. Origin of fines is also influencing their properties, which makes it almost impossible to make comprehensive statements about fines. Niskanen published in 2008³ some general differences, considering pulping process as well as further processing steps. In addition, origin and morphological data are measured and compared. Research on fines separation between mechanical and chemical pulping is of utmost importance for papermaking industry (Tab. 3.). Further differences can be observed between primary and secondary fines.

Table 3 Structural property differences between mechanical and chemical pulp.³

Property	Mechanical pulp	Chemical pulp
Yield on wood	High	Low
Amount of lignin	High	Low
Amount of hemicellulose	High	Low
Charge in water suspension	More anionic	Less anionic

Fines content	High	Low
Long fibers per unit mass	Few	Many
Surface area	High	Low

All differences in characteristics are accompanied by structural differences (Tab. 4). This can be determined in fiber structures as well as in structures of fines. An additional factor is that shorter fibers own a higher surface area to create hierarchical structures leading to better bonding abilities. Variations of process steps are a further reason, additional steps can increase (e.g. grinding) or lower (e.g. bleaching) the amount of hemicellulose and lignin influencing the pulp and final product.

Table 4 Comparing fiber specific properties between mechanical and chemical pulp

Property	Mechanical pulp	Chemical pulp
Fines structure	Lamellar	Fibrillar
Bonding ability of fines	Good	Excellent
Fiber structures	Stiff, coarse, straight	Slender, curly, kinky
Fiber shape	Short and wide	Long and narrow

In recent years' research concentrated on the influence of lignin in pulp, which might be also an important factor due to improved bonding through the higher amount of hydroxyl groups. It would be also interesting to vary lignin amount into a fines slurry to achieve higher interactions between hydroxyl groups.

1.2.5. Composites with fines

Hierarchical structures increase the surface area and might minimize the pore sizes, depending on the pore size of the second substance. Furthermore, the density is increased by filling free space with smaller particles. The aim is to achieve higher surface area and smaller pore size retaining wider channels, which are important for fast charge/discharge processes.

2. Supercapacitors

Supercapacitors are a booming research field, because they are a serious alternative to batteries with the advantage of delivering much higher power albeit for only a short time. They are the technology of choice to shave peak power demands of battery devices like notebooks, cell phones or sliding doors. If devices run out of electricity, supercapacitors can deliver the energy to save data, or to open emergency exit doors. Other uses for energy recuperation for example in stop and go traffic. Trams and cars are able to generate energy by braking, which can be stored and used for acceleration.

2.1. Working principle

Supercapacitors are highly reversible energy storage devices that can store electrical energy for a specific time. Energy losses can appear during charge and discharge by Ohmic losses and through self-discharge, which are both depending on electrode materials and electrolyte. In comparison to batteries, supercapacitors can deliver charge much faster. However, the specific energy is smaller (Wh/kg). Figure 15 depicts advantages and disadvantages of various energy storage devices.

The prime cause for very fast storage rates and high cycle life is that EDLC's store charge by electrostatic adsorption of ions at the ion/electron conductor interface. This way they do not have to exchange charge over this interface in Faradaic reactions like in batteries. Faradaic reactions are associated with activation overpotentials and as such much more limited in rate than electrostatic processes. Therefore, EDLC's do not have an activation overpotential making the storage systems highly repeatable and faster compared to systems based on redox reactions. The minimization of the limitation due to Faradaic mechanisms increases the contribution due to Ohmic resistance. Focusing on current collectors and cell construction improves the conductivity of the media and improves cycle life. The high conductivity of metals has the advantage to minimize energetic losses; main contributors to the overall resistances are therefore carbon and the electrolyte.

Differences between batteries and supercapacitors are based on the used materials since they affect the storage mechanism. Batteries store energy by redox reactions, whereas carbon based supercapacitors store energy within an electric double layer (EDL). Therefore, as the

electrode is polarized ions from the electrolyte accumulate at the surface of the electrode, building an EDL. The amount of accumulated ions is proportional to the electrical charge. Two space charge zones can be observed, one at the electrode and the other through the ions in the electrolyte. Figure 7 depicts a classical supercapacitor and Fig. 8 the storage mechanism used for EDLCs due to ions in the electrolyte.

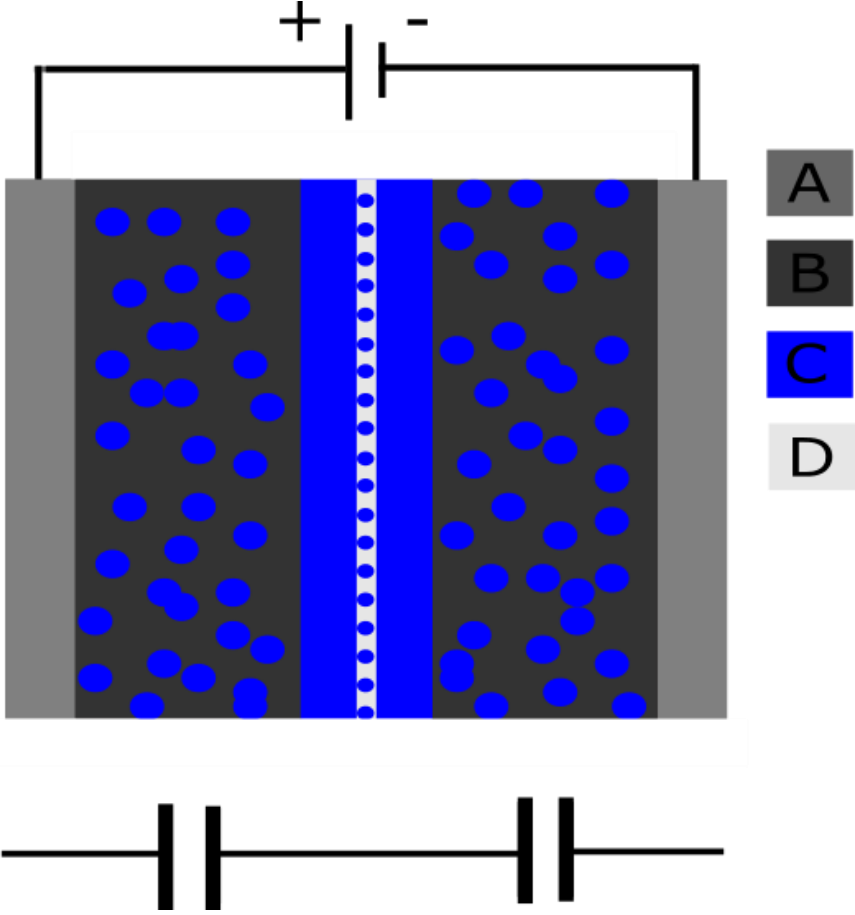


Figure 7 Illustration of a supercapacitor A) Is aluminum to stabilize the electrode material B) the highly porous electrode material, where pores are filled with C) the electron conducting electrolyte. D) Membrane to avoid contact between both electrodes, which will lead to a short cut of the supercapacitor. Below the capacitor is the equivalent electrical circuit of the supercapacitor, which are two serially connected capacitors.

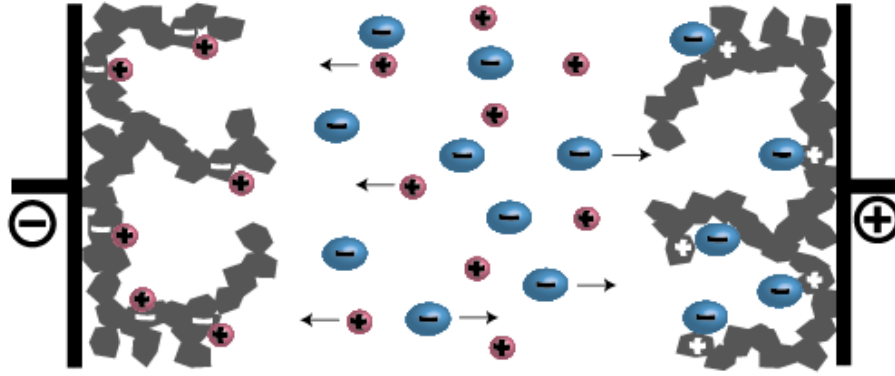


Figure 8 Scheme of an EDL storage illustrating the formation of a double layer.¹³

In 1853 von Helmholtz introduced the theory of the electrochemical double layer where ions accumulate in close proximity to the electrolyte interface.¹⁴ It was only in 1957 when this could be first exploited to store energy. Equation (1) dates back to *von Helmholtz's* publication, where C denotes the capacity (in F), epsilon ϵ the dielectric constant of the electrolyte, A the surface area of the electrodes and d the distance in between. In conclusion, capacity is directly depending on surface area and the distance between both electrodes. The higher A and smaller d the larger is the final capacity. The preferred distance between these electrodes should be around a few Ångstroms.¹⁵

$$C = \epsilon \frac{A}{d} \quad (1)$$

The earliest accepted change was introduced by Stern, he combined the *von Helmholtz* model with more advanced theories in 1924¹⁶

He introduced the theory to separate the double layer capacitance C_{dl} in two different regions, namely the compact double layer capacitance (C_H) and the diffusion region capacitance (C_{diff}). A reciprocal dependency between the capacities is noted in Eq. (2). The capacity of the supercapacitor is principally limited by the electrode material, especially by the ion accessible surface area. Further limitations originate from the electrolyte/solvent system, where the polarity and the size of ions play a crucial role.

$$\frac{1}{C_{dl}} = \frac{1}{C_H} + \frac{1}{C_{diff}} \quad (2)$$

Basically, supercapacitors store electricity in the same way like standard capacitors. Main differences stem from highly increased surface area due to activated carbon and very thin

electrical double layers between electrolyte and both electrodes. As depicted in Fig. 7 supercapacitors behave like two serially connected capacitors.

In a symmetric supercapacitor, both electrodes behave like equal, serially connected capacitors. The dependency between the capacity of single electrodes and the total capacity (C_{Cell}) is in Eq. (3). C_+ indicates capacity of the positive and C_- of the negative electrode. The equation can be simplified for symmetric supercapacitors with the same loading for both electrodes. Eq. (4) denotes the capacity of both electrodes (C_E) and the dependency to the total capacity (C_{Cell}).

$$\frac{1}{C_{Cell}} = \frac{1}{C_+} + \frac{1}{C_-} \quad (3)$$

$$C_{Cell} = \frac{C_E}{2} \quad (4)$$

Stored energy E is determined by the square of the maximum operating voltage V_{max} and the capacitances of the negative (C_-) and the positive C_+ electrodes (Eq. 5).

$$E = \left(\frac{C_- C_+}{C_- + C_+} \right) V_{max}^2 \quad (5)$$

Balanced electrodes simplify the equation to

$$E = \frac{1}{2} C \cdot V_{max}^2 \quad (6)$$

The dependency of the charge Q is given by

$$Q = C \cdot V \quad (7)$$

Relating to the power by

$$P = \frac{V^2}{4R} \quad (8)$$

The resistance R is the series resistance of the device, multiplied with the factor 4 exhibits the importance of it. Furthermore, the benefit of higher voltages is shown in Eq. 8.

The parameter limiting the power is the internal series resistance (ESR). The ESR can be divided into the electronic resistance of the electrodes, the diffusion resistance (diffusion ions in the smallest pores) and the ionic resistance of electrolytes. Material impurities will further increase the resistance.

2.2. Electrode materials

Electrode materials also determine the storage mechanism of the supercapacitor; this has a large impact on properties and performance. The different types of supercapacitors classified by storage mechanisms are shown in Fig. 9. ECDL's store energy via adsorption and are therefore highly reversible. Pseudocapacitors are based on fast redox reactions at the electrode surfaces similar to batteries. The third class consists of hybrid supercapacitors using both storage mechanisms. All storage techniques used in supercapacitors are exhibited in Fig. 10, deepening the electrochemical differences between batteries and supercapacitors.

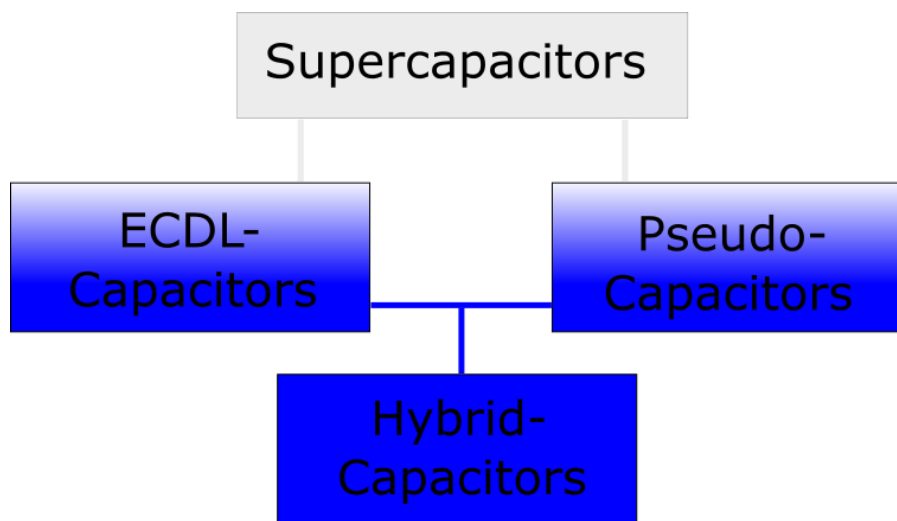


Figure 9 Overview of supercapacitor types classified by storage mechanisms

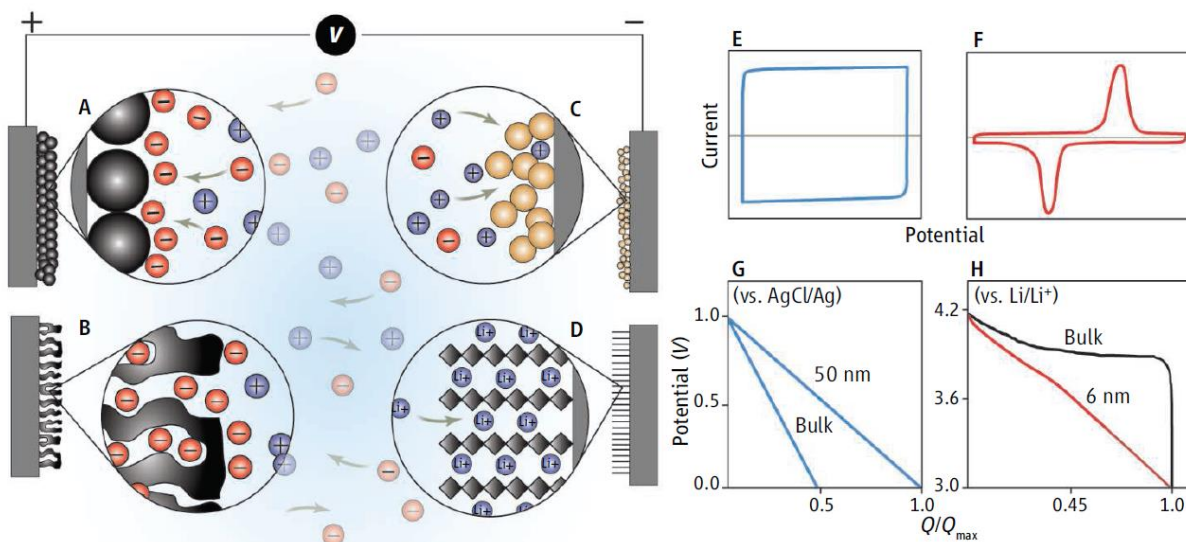


Figure 10 (A to D) Illustrates different storage mechanism in SCs. (A) shows the electrostatic storage at carbon particles and (B) in pores. Pseudocapacitive energy storage via inorganic materials is exhibited in (C) (e.g. RuO_2). (D) stores energy by intercalating Li^+ . (E-H) compares supercapacitors with batteries. The linear potential change in (E) is typical for all SCs, while batteries show peaks of redox processes (F). The approach of batteries to SCs is depicted in (H) by using nanoscale battery materials.¹⁷

EDLC's are double layer capacitors, where energy is electrostatically stored in activated or nano-formed carbons. Using this system provides plenty of advantages such as very high cycle rates and combustible electrode materials. Further, these systems are very economic when combined with aqueous electrolytes.

Two different types of electrodes are using electrochemical storage processes. Metal oxides like $\text{RuO}_2 \cdot n\text{H}_2\text{O}$ are very expensive compared to cellulose based electrodes, but intercalation of H^+ inside the amorphous structure and high capacities caused through low ESR makes them very interesting. However, these systems are restricted to aqueous electrolytes. Secondly, electronically conductive polymers can store energy electrochemically. Ready availability, cheap prices and highly porous structures make the application of cellulose (derivatives) in this field very appealing. In the past, the cycle rates of polymers (polyaniline^{10,19,20}, polypyrrole^{21,22}, or polythiophene) have been increased but still do not reach current requirements for EDLC's. Recently published papers specified losses of 4.8% over 5000 cycles²². Pseudocapacitors might be a storage media of the future.

Hybrid electrodes combine both storage effects by assembling asymmetric electrodes. One of the electrodes is charged via redox reactions or by redox active molecules in the electrolyte,²³ whereas the other electrode electrostatically stores energy.

2.3. Most common supercapacitors

2.3.1. Electrochemical Double Layer Capacitor

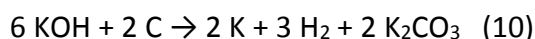
Carbon based electrodes use EDL to store energy for reaching very stable cycle rates and inexpensive use of side and waste products. In order to avoid competition between agriculture and industry, most publications concentrate on biological waste like potato peel, or corn leaves. Plenty of products have already been investigated in literature ranging from classical biological waste^{24,25,26,27}, alternative ways to utilize overproductions²⁸ to specially synthesized carbon compounds. 2000 m²/g or even higher surface area have been reported as ideal parameter for supercapacitors. Paper surface area is typically measured to be 100 times lower. Therefore, an activation process must be performed prior to electrode fabrication. Different activation methods influence pore size and surface area. Oxygen, CO₂ or nitrogen are predominantly applied for activation of carbon. The use of heteroatoms increases the attraction of the surface to electrons, therefore higher amounts of electrons can be stored and capacitance is improved. These additional effects (pseudocapacitive effects) accompany the electrical double layer mechanism.

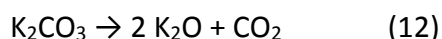
Oxygen

Different activation processes enable the incorporation of oxygen into the activated cellulose. A promising route is to exploit the Boudouard reaction for cellulose doping. It shows the equilibrium between CO and CO₂ in direct relation to temperature at 800°C the prevailing amount is CO (9). Avoiding burning of cellulose, carbonization is accomplished in inert gas.



Recently, most carbons have been activated by KOH. Here, a mixture of KOH and precarbonized cellulose is prepared. During activation, a gasification process takes place. KOH is reduced during heating by carbon to potassium and K₂O²⁹. Carbon reacts with oxygen to CO and CO₂. Since 800°C is the boiling temperature of potassium, the reaction starts at this point. Pores are formed by diffusion of gases into cellulose, Eqs. (10-12). Furthermore, the diffusion yields in the doping of the cellulose. Higher temperatures narrow and close pores, therefore it is important to test different temperatures for carbonization.





Nitrogen

Nitrogen doping is a promising path of activation.^{30,31,32} Doping enhances the charge density by interactions of protons with nitrogen. Doping with elements distinguished with higher electronegativity increases polarity of the activated cellulose. Possible paths are either to form lattice nitrogen (N is substituted to carbon) or chemical nitrogen (functional groups). Two possibilities are accomplished, namely pre doping and post doping. Post doping shows lower amounts of nitrogen, but the whole process is easier to carry out. Ammoxidation identifies the process employing ammonia based chemicals for post doping. Typical methods for predoping are carbonization of nitrogen containing polymers (PAN and polyvinylpyrrolidone) and steam activation.

2.3.2. Pseudocapacitors

Using polymers to realize pseudocapacitors offers many advantages like easy preparation, flexibility and low cost/weight. Conductive polymers are enwrapping cellulose in a thin film. Reversible redox reactions store energy in this polymeric coating. Through alternating single and double bonds a conjugated π -system is built leading to a continuous backbone of sp^2 hybridized carbon centers. Suitable oxidants lead to electron deficiency. Striving for electroneutrality, ions are taken up, so called p-doping. Nowadays, most of conductive polymers are p-doped. Whereas EDLC store energy electrostatically, pseudocapacitors utilize the volume. Varying p- and n-doping for electrode materials result in different possibilities for asymmetric supercapacitors. Full oxidation of the positive electrode and a neutral negative electrode will reach a potential difference of 0.5 - 0.75 V. Polymeric coated templates operate only in aqueous electrolytes.³³

Most publications focus on polyaniline (PANI)^{20,34,35}, polypyrrole (PPy)^{22,29} and polythiophene. Low prices, easy handling and availability are the main reasons to utilize polymers as a serious alternative to classic EDLC supercapacitors. Furthermore, in the last years cycle stability could be enhanced, but still falls short of the stability of pure EDLCs. Pseudocapacitors are not only

redox-active, they also store energy by adsorption. They are combining both effects thereby increasing the capacity.

Polyaniline

Polyaniline is polymerized through electrochemical or chemical oxidation of aniline (Fig. 11).

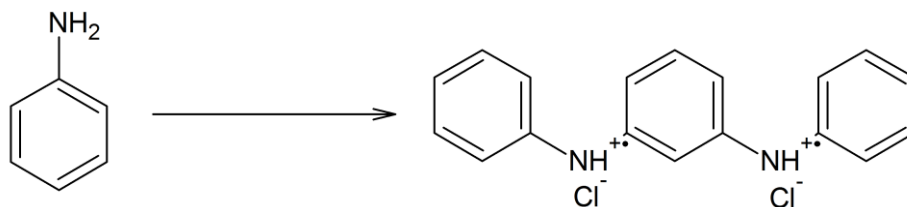


Figure 11 A fundamental scheme of the polymerization of aniline, which reacts to polyaniline.

During the synthesis, emeraldine is formed (Fig. 12). Basic media is used to transfer the acidic emeraldine into an alkaline form. Delocalized radicals are stabilized by the ring system. Radicals are the reason for the high conductivity of emeraldine salt, otherwise high conductivities would be rather low. Since polyaniline has many oxidation states, it is of utmost importance to synthesize the conductive state. Neutral emeraldine is a perfect insulator with 10^{-10} S/cm. Specific capacitance up to 200 F/g are possible by chemical preparation. PANi has good cycling stabilities, nevertheless during charging mechanical failures appear and reduce the capacity.

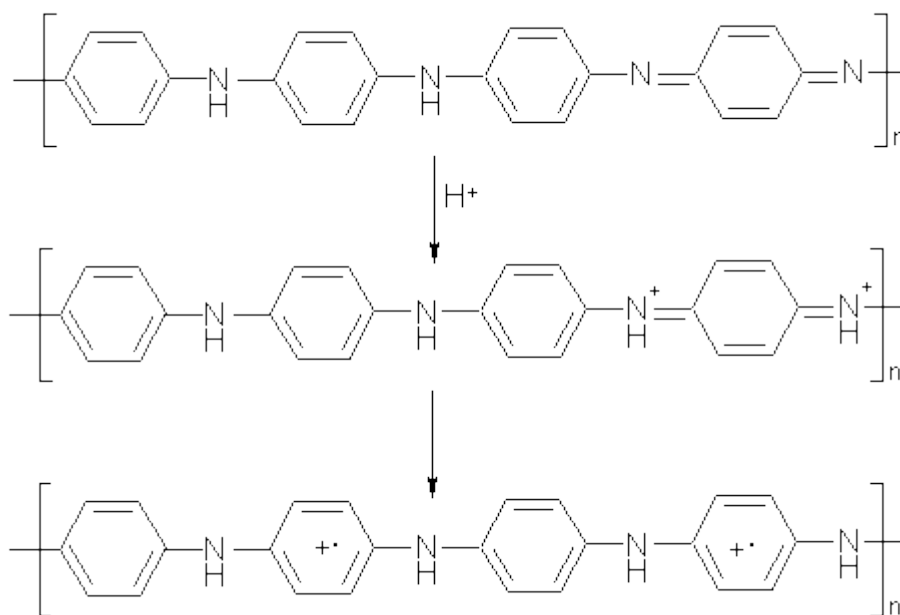


Figure 12 Reaction scheme to synthesize the green emeraldine salt (conductive state) starting with polyaniline

Polypyrrole

Polypyrrole is the second most important conductive polymer on the market (Fig. 13).

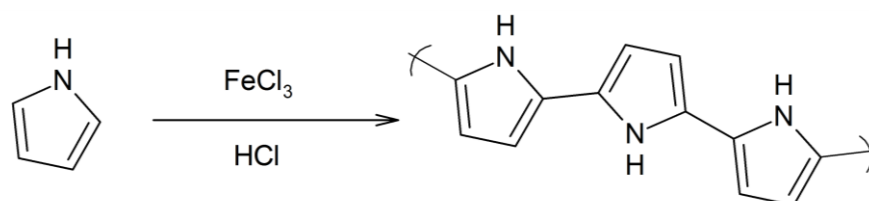


Figure 13 Polymerization of polypyrrole via anodic oxidation

Depending on synthesis, every third or fourth unit is charged (Fig. 14). It is the most promising polymer on the market, since it is air-stable over months. PPy based materials are expected to exceed PANi composites in future. Predicted capacities range from 100 to 500 F/g. Special attention should be paid to the thickness of the electrode. Thinner electrodes reveal higher capacities. However, a major disadvantage is the cycle life, due to high losses (40% after 4000 cycles).²²

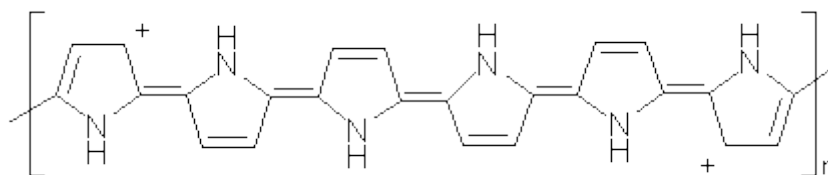


Figure 14 Doped polypyrrole, which results in higher conductivities.

2.4. Components

2.4.1. Separator

As already mentioned, separators avoid contact between the two electrodes in supercapacitors. It has to be thick enough to avoid contact, but thin enough not to add too much resistance, weight and volume.

2.4.2. Electrolytes

The electrolyte is a liquid ion conducting and electron insulating material in a supercapacitor. Additionally, they need to be stable and inert. The stability over a wide potential range is of utmost importance, which has been explained above. Based on this dependency literature concentrates on organic electrolytes exhibiting much higher ranges. Whereas aqueous electrolytes are limited to practical values close to 1 V, organic ones point out with 2.5-2.7 V. Aqueous electrolytes concentrate on acids (e.g. H_2SO_4), bases like KOH and salts (e.g. NaClO_4). Typical concentrations start at one, reaching up to several molar. Representative organic solvents are acetonitrile, propylene carbonate and tetrahydrofuran containing conductive salt, predominantly alkaline and tertiary alkylammonium cations with BF_4^- anions. Further investigations concentrate on ionic liquids as electrolytes with the advantage of solvent free assembling.

TEABF_4 in acetonitrile (ACN) as example is one of the best conducting salts with up to 60 mS/cm. Aqueous systems conduct about 20 times better than organic media³⁶. Furthermore, capacities are much higher for aqueous systems than for organic ones. However, the electrolysis of water is the major disadvantage. Further differences are variations in ion sizes, because organic electrolyte salts are larger than aqueous one. The ideal pore size for TEABF_4 in ACN is 0.76 nm at the negative electrode and 0.68 at the positive.³⁷ Ion size and the perfect

pore size correlate with each other. Aqueous electrolytes are smaller in size thus also minimizes the favorable pore size. Highest reported capacities with H_2SO_4 as electrolyte are at a pore size of about 0.53 nm for KOH it would be even smaller.³⁸

2.5. Supercapacitors and other energy storage possibilities

The Ragone plot shows graphically ranges for typical energy storage devices with regard to specific energy and specific power (Fig. 15). The higher specific power indicates higher current peaks in short time, but specific energy is about ten times shorter than for batteries. The diagonal lines indicate characteristic discharge times.

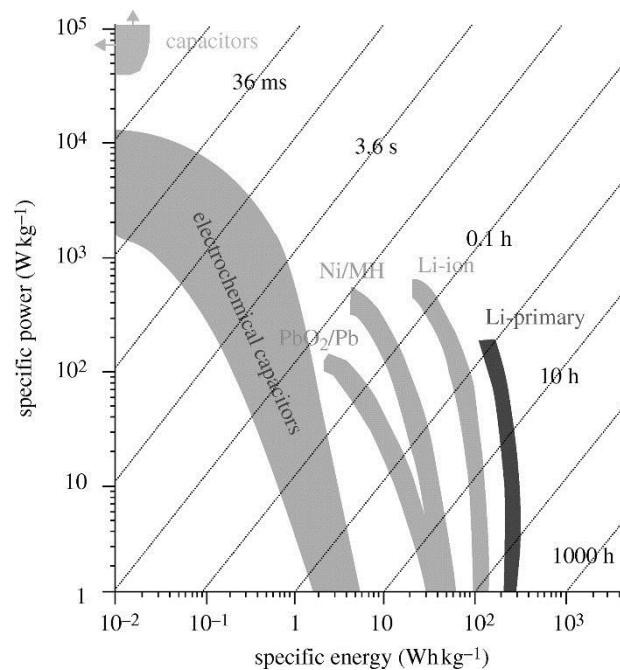


Figure 15 Ragone plot compares different energy storage systems with each other due to specific power to specific energy.³⁹

3. Electrochemical methods

Supercapacitors can be either tested in 2- or 3-electrode setups and were tested in either case in Swagelok® test cells. When a reference electrode was used, the 3-electrode cell was equipped with a partially delithiated $\text{Li}_{1-x}\text{FePO}_4$ reference electrode (RE). $\text{Li}_{1-x}\text{FePO}_4$ exhibits a constant potential of 3.45 V vs Li/Li+. When employing a RE it becomes possible to probe the behavior of a single electrode. For example, it is possible to see the deflection of the single electrodes from the open circuit potential (OCP) when the total cell voltage (positive electrode vs negative electrode) is controlled. This way for example both imbalanced electrodes as well as different anion and cation adsorption capacitances can be seen. Figure 21 specifies the wiring of the Swagelok® cell.

Typically, symmetric devices are tested, i.e., CE and WE are made from the same material; consequently the OCP between the two electrodes will be close to zero. Their potential with respect to the NHE RE will be normally close to 0 V, which is around 3 V vs Li/Li+ due to the reversible potential of typical surface groups on the carbon. Uncharged, the voltage difference between a $\text{Li}_{1-x}\text{FePO}_4$ RE and the WE/CE will therefore be ~ 0.45 V.

To keep the potential deflection of either electrode within the thermodynamic stability of the electrolyte (applicable voltage window) the electrodes need to be properly balanced.

Higher deflection of the potential on one electrode is the result for differences in loading, because the lower loading has to be compensated by higher deflections. The vertex potential was set lower than 2.5 V, avoiding the decomposition of ACN. Very brittle materials are affected easily, predominantly resulting in a loss of mass from the active material. The material is highly electrostatic and very light, which makes it hard to handle.

3.1. Cyclic voltammetry

Cyclic voltammetry is a controlled potential technique where the current in response to deflection of the working electrode potential from OCP is measured. Thus, the current in response to the driving force (overpotential) is obtained. The voltage is deflected with fixed scan rates dU/dt between the upper and lower cut off voltages. For SCs CVs are used to measure

- Specific capacitance, power and energy

- Cycle life and degradation
- Possibly determining redox processes overlapping with the capacitive storage process

In an ideal capacitor the capacitance is independent of voltage, which is why a rectangular shape in the CV is obtained with the current being

$$i = C \frac{dU}{dt} \quad (13)$$

Fig. 16 depicts a classical CV of a supercapacitor, where current density is plotted versus cell voltage. Normalizing the signal by dividing through the scan rate yields the specific capacitance via

$$C = \frac{I}{\frac{dU}{dt}} \quad (14)$$

Deviations from the rectangular shape arise from the resistivity of the system, that can in the simplest case be regarded as a parallel connection of a capacitor and a resistor.

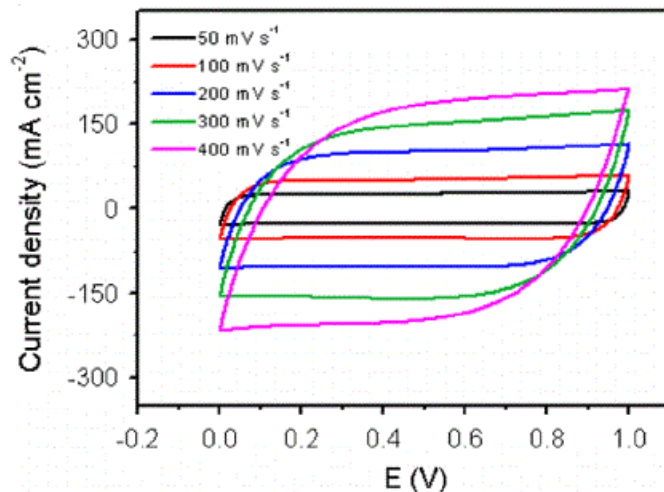


Figure 16 Cyclic voltammometry signals. (a) Image of a CV, current is almost rectangular, means voltage independency.⁴⁰

3.2. Galvanostatic cycling

Galvanostatic cycling is a controlled current technique where the potential is recorded as a function of time. Plotting potential versus time for an ideal supercapacitor gives a triangular shape, Fig. 15. The same parameters can be determined as in CVs

- Capacitance
- Cyclability
- Resistance

In galvanostatic measurements, capacity is direct proportional to current I , further factors are charge or discharge time Δt and the voltage window Δu (Eq. 15).

$$C = \frac{I \cdot \Delta t}{\Delta u} \quad (15)$$

For inversed or interrupted cells, voltage drop u_{drop} and the current Δi are directly related to cell resistance R (16).

$$R = \frac{u_{drop}}{\Delta i} \quad (16)$$

By repeating measurements over a set number of cycles, it is possible to determine cyclability. Variations of the current mainly affects the time for charging/discharging the supercapacitor (Fig. 17). Slower charging is mostly accompanied by slightly higher capacities. With time, further ions adsorb on the surface of the electrode, yielding in higher capacities. Therefore, capacity differences can be observed for different currents.

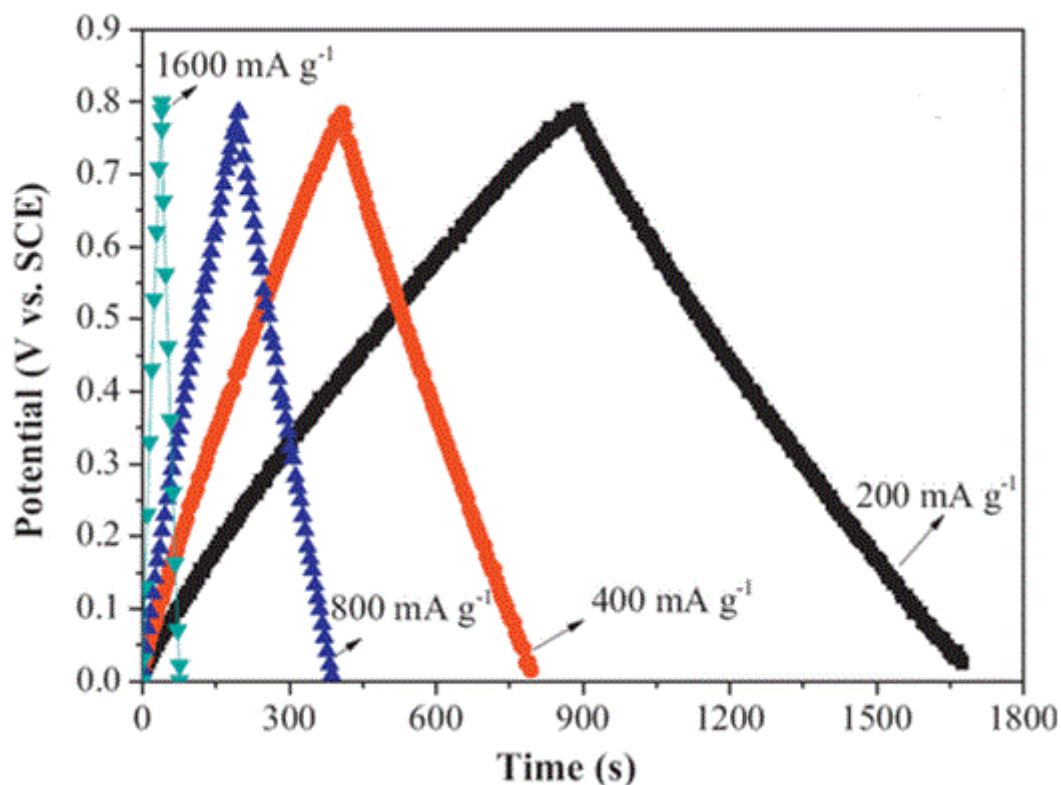


Figure 17 Typical galvanostatic measurement illustrates dependency between current rate, voltage and time for charging^{A1}

3.3. Electrochemical Impedance Spectroscopy

EIS is used to determine frequency dependent response of a sample towards a sinusoidal perturbation. For the case of sinusoidal current I being applied onto a system the voltage response V is given by

$$V = Z * I \quad (17)$$

With Z being the complex impedance $Z(\omega) = Z_{Re} + j Z_{Im}$.

The Randle equivalent circuit (Fig. 18) can approximate an electrochemical system. The series resistance R_s is serial to the parallel circuit including C_{dl} the double layer capacitance, parallel to Z_w the diffusion impedance and R_{ct} , which is the charge transfer resistance.

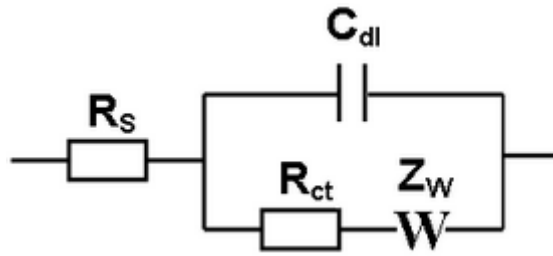


Figure 18 Randles circuit is an equivalent electrical circuit, used for EIS measurements

Different types of electrodes are easily distinguishable. Pseudocapacitors show a loop at high frequencies, increasing linearly in low frequencies (Fig. 19). EDLCs are totally linear, therefore R_s and C_{dl} are dominant in Randles circuit for EDLCs.

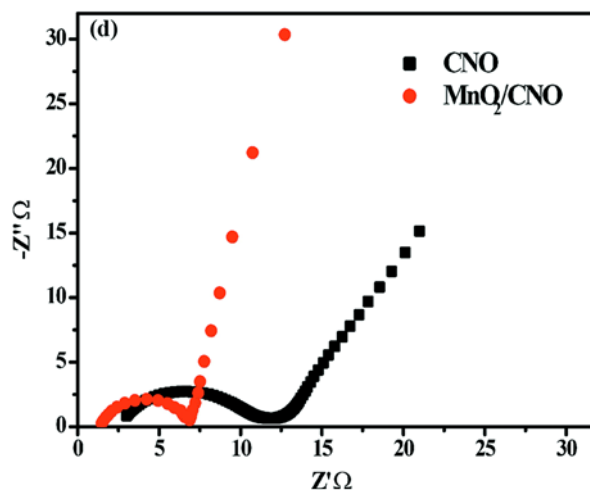


Figure 19 Impedance measurements of pseudocapacitors with the typical loop at higher frequencies⁴²

Resistivity of the whole device is one of the most important parameters for SC power. For 1 M TEABF₄ in acetonitrile 57 mS/cm are measured and higher concentrations improve conductivity slightly.

3.4. Self-discharge and leak current

Self discharge is a measure of the voltage drop at open circuit after the device was charged to a certain upper cut off voltage. In SCs this can amongst other process be caused by rearrangement of charge carriers as well as slow electrolyte oxidation if the device is charged to high voltages.

Leak current is a measure of parasitic current by holding the cell voltage at the upper cut-off potential and recording the current. The current is recorded during charging the supercapacitor, afterwards it decreases to a constant plateau, which is the leak current.

Both parameters are very important using redox active electrolytes, but it is also desirable to report them for pure EDLCs.

4. Analytical methods

4.1. Inductive Coupled Plasma Mass Spectroscopy (ICPMS)

Inductive Coupled Plasma Mass Spectroscopy is a sensitive device deployed to verify traces of elements in the paper pulp. Ionization of argon through high frequency current and heating the sample up to maximum 10.000°C ionizes atoms. This results in a plasma, ions are accelerated by an electrical field to an analyzer. There all ions are measured, detected, and assigned by the system.

It is a modern possibility to prove almost all elements in the periodic table, up to nanogram per liter. Especially the linearity over a wide range (Nanogram to gram) is highly considered. The trace analysis was performed by an ICPMS (Agilent 7500ce unit). Fines were digested in nitric acid before analyzation.

4.2. Brunauer–Emmett–Teller (BET)

Since the capacitance of SC electrode materials is determined by the ion accessible surface area the specific surface area is a highly important parameter to be determined. Albeit not exactly the same, the surface area accessible by adsorbing gases is a good measure. Therefore, N₂ adsorption measurements were performed that yield the specific surface area when evaluated by the Brunauer–Emmett–Teller method (BET). The measurements give specific surface area, pore size distribution and pore volume.

Multi and single point measurements are common for BET. Multi point measurements are calculated via the adsorption isotherm equation. Single point measurements determine the surface area either by volumetric gas adsorption or dynamic flow gas adsorption.

Surface area and porosity were analyzed by a TriStar II from Micrometrics. The specific surface area was calculated using the Brunauer-Emmett-Teller (BET) and Langmuir equation. Before measuring the samples, they were degassed with nitrogen at 120°C overnight. As alternative, polymeric samples were dried under vacuum at 23°C. Conditions depended on the sample. Polymer coated samples were dried at room temperature to keep the structures.

4.3. Scanning electron microscopy (SEM)

SEM is an imaging system based on electron microscopy, a focused electron beam is scanning the surface of a dry vacuumed sample. Interactions of electrons with atoms in the bulk results in an image. The ratios on the image illustrate the proportion between scanned surface and the monitor. Electrons from the beam come from an electron source, like Wolfram wire. By heating it up electrons, get emitted and accelerated by an electrical field. Magnetic coils focus the beam and control the scanning of the surface. The beam mainly consists of primary electrons, which are not imaging. Accountable for imaging are secondary electrons, generated through collisions between atoms and primary electrons. Different types of electrons can be allocated, detectors recognize the energy of electrons and refer them. In classic SEMs, only conductive samples can be investigated.

We measured our samples with so-called low voltage electron microscopy (LVSEM), a more particular technique. Reducing the depth of penetration, compared to classical SEM`s. The main difference is the beam energy, LVSEM has its maxima at 5 keV, whereas normal SEM goes up to 30 keV. Lower beam energies decrease penetration depths, which causes less volume and more specific investigations in the surface of the specimen. Higher penetration depth increases the analyzed volume. On the other hand smaller depths higher the resolution and improve visualization of nanopores.

Furthermore, it enables investigations in non-conductive materials. This is only possible due to a special effect, the number of incoming and emitted electrons have to be the same. This avoids unwanted charges on the sample surface. Otherwise, specimens have to be coated and layers even in nm range can distort the result, especially by measuring nanopores. A further advantage is that it can be investigated in real surfaces, neglecting bulk.

Fischer`s paper⁴³ indicates that much more details can be seen by using LVSEM compared to HVSEM measurements.

4.4. Energy-dispersive X-ray spectroscopy (EDX)

Energy-dispersive X-ray spectroscopy is an elemental analysis technique of solid samples. Principally the measurement system is based on characteristic atomic structures and unique emission spectra for each element. The type of excitation is equal to SEM, a beam is directed onto the vacuumed sample. Charged particles may interact and excite an electron from the inner shell, if the energy of the particle is sufficiently high, the electron is ejected forming an electron hole. Thus, an electron from an outer shell fills the hole. The energy difference of both electrons is released in form of element specific X-rays, detected by an energy-dispersive spectrometer. On account of the intensity, quantifications of the element are possible, considering all elements allow reporting the composition of the sample.

All samples analyzed by EDX were fixed on a double sided adhesive copper tape, quantitative determination has been performed with an EDX VEGA II from Tescan.

4.5. Infrared Spectroscopy (IR)

Infrared spectroscopy is a fast, cheap and precise method to prove the progress in carbonization, measuring the reduction of functional groups on the cellulose. Using the infrared region for analysis, different absorptions spectra can be observed. Functional groups are interacting with the light and change the spectra compared to the blank recorded in advance. Infrared light has longer wavelengths than visible light, which is going along with lower frequencies. It is sensitive to functional groups of molecules detecting rotation and vibration. Those changes are the absorbance plotted on the y-axis versus reciprocal centimeters on x-axis. The frequency ranges from $14000\text{-}10\text{ cm}^{-1}$ ($0.8\text{ }\mu\text{m} - 1\text{ mm}$ wavelength). Most common is Fourier Transform Infrared Spectroscopy (FTIR) because all kind of phases (gas, liquid, solid) can be investigated.

All experiments were performed in an ALPHA FT-IR spectrometer from Bruker. For the measurements an attenuated total reflection (ATR) attachment was used with 48 scans at a resolution of 4 cm^{-1} and a scan range from $400 - 4000\text{ cm}^{-1}$. The data were analyzed with OPUS 4.0 software.

5. Materials and Methods

All chemicals used were >99.0% pure, otherwise it is declared in the procedure. HCl (37%) and KOH (85%) have been always purchased from VWR Chemicals.

5.1. Preparation of chemical pulp

Fines content in chemical pulp was about 2.92 to 6.32 wt% and in thermomechanical 23 to 25 wt%.⁶ The separation of fines from paper pulps was done using a house made device consisting of following elements

The pulp in a barrel was diluted with distilled water and pumped towards the pressure screen. Fast turning blades fed pulp in the perforated strainer (exterior wall replaced by an aluminum strainer), with hole sizes below 100 μm . The fast rotations washed fines into the “accept flow”, from there they were pumped into a second barrel. The rest of the pulp exited on the reject flow and went back into the pulp barrel, so pulp was washed several times (Fig. 18). Separated fines were highly diluted; therefore, it was necessary to increase the amount of fines using floating mechanism.

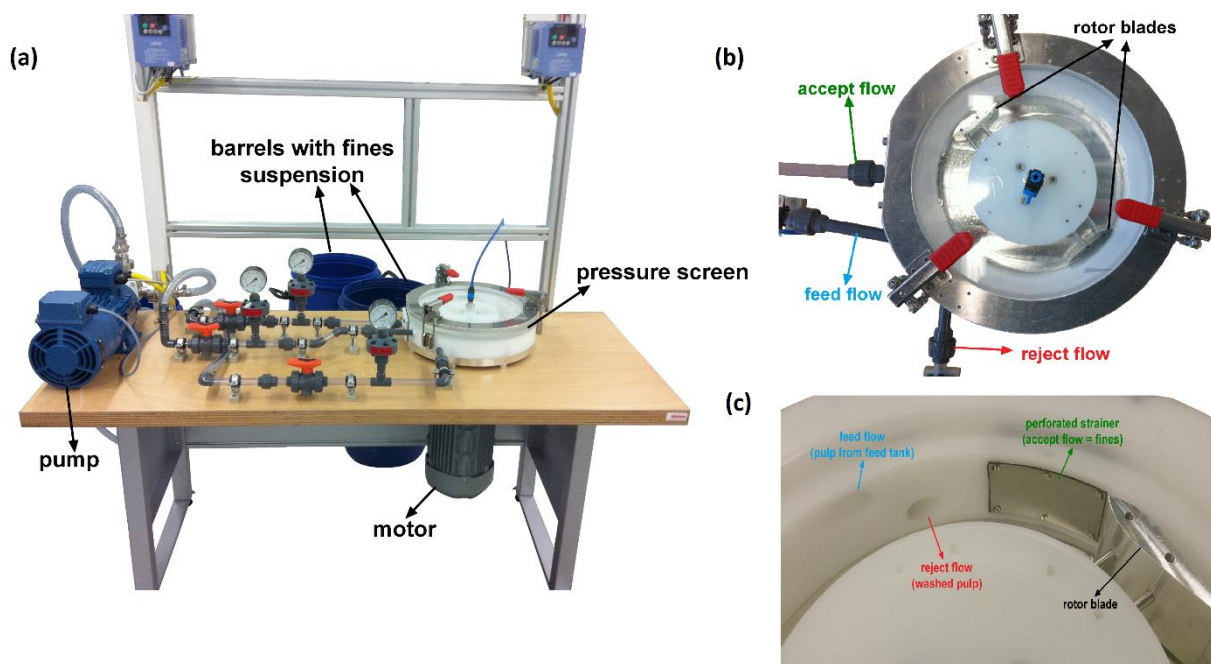


Figure 20 Equipment to separate fines from the pulp. (a) shows the whole process starting by pumping diluted pulp out of the ton into the pressure screen, where fines get separated. (b) is an overview of the pressure screen with one inlet and two outlets. (c) is an inner view of the pressure screen, rotor blades are turning a pressing pulp against the perforated strainer, so fines can be separated. Copyright Wolfgang J. Fischer (TU Graz)

The fines were dried by lyophilization (-52°C ; 0.062 bar). All in all, a total amount of 4.06 wt% fines have been obtained in the suspension. A Christ Alpha 2-4 LD freeze dryer was keeping the supramolecular structure of fines.

5.2. Activation process of fines

Carbonized fines were activated in different ways to compare activation processes with each other. All processes were listed in Tab. 5. For better comparability, all activation processes were proceeded with the same type of primary fines.

Table 5 Comparing different activation types for fines

Activation	Type	Temperature	Comment
1	Primary	150°C	Activation in the microwave with 1 M KOH ⁴⁴
2	Primary	800°C	Activation by mixing with NaHCO_3 ⁴⁵
3	Primary	800°C	Activation by grinding with KOH ⁴⁶
4	Primary	800°C	Activation with KOH, without grinding ⁴⁶
5	Primary	800°C	Without activation

Microwave assisted activation:

All microwave assisted synthesis was proceeded in a Biotage Initiator EXP EU. Sample 1 was synthesized in a vessel approved for 2-5 mL. A mixture of 1.5 g suspension (4.06 wt% fines) was added to 1 mL distilled water containing 60 mg KOH. The solution was heated up to 120°C (high absorption) and kept constant for 10 minutes, stirring the suspension steadily.

Activation by carbonization

Lyophilized fines (-52°C; 0.062 bar) were precarbonized in a tube furnace (TZF 15/610 from Carbolite) at 400°C. It was evacuated and filled with argon; this procedure was repeated three times in a row. A steady argon stream avoided combustion of the fines.

Sample 2 was activated by sodium bicarbonate (VWR Chemicals). Precarbonized primary fines were mixed with NaHCO₃ with a ratio of 1+3 250 mg of precursor were used per charge. After manual milling, the mixture was heated to minimum 800°C. All carbonization steps were accomplished in an inert gas phase using the implementation as described above.

After cooling down to room temperature, the solid mixture of activated carbon (Potassium oxide and potassium) was stirred in 10 vol% HCl (VWR Chemicals), which is added dropwise to a ratio of 1+99. After adding HCl, the solution was stirred for 5 hours to complete the reaction. Solid particles were separated by centrifugation. The activated cellulose was diluted with distilled water and centrifuged. This procedure was repeated three times in a row. All centrifugation steps were performed with 4000 rpm at a temperature of 13°C. The activated carbon was dried at 50°C under vacuum.

Sample 3 and 4 were treated the same way, grinding and activating cellulose with KOH. Furthermore, sample 4 was not milled, but all other process steps were equal.

Sample 5 included grinding, but without activating materials, all other process and washing steps were the same.

We proceeded with KOH and tested the influence of grinding and the difference between primary and secondary fines.^{47,48} Grinding together with already carbonized fines equals well distributed alkaline in precarbonized fines.

5.3. Composites with fines from wood

House made cellulose nanocrystals (CNC`s) were used to manufacture highly hierarchical wooden composites. Table 6 lists the compositions of the composites. Cavities through fines can be used for storing nanocrystals, achieving much higher surface area than BET has been estimated for fines. It would expected to be hierarchically structured to optimize surface area and channels.

Table 6 Composites of fines with CNCs to increasing the surface area proved via BET.

Sample	CNC [g]	Fine [g]
1	2	2
2	0.4	3.6
3	3.6	0.4

Blending before freeze drying enables an excellent distribution of CNCs in fines. All other steps were processed like specified before.

5.4. Fines from wood coated with conductive polymers

Polyaniline

Polyaniline was synthesized as reported in literature from Wang¹⁹. 1 g of fines was diluted with 125 g of water, 1 mL aniline (freshly distilled) (Fluka) and 62 g dimethylformamide (DMF) (Sigma-Aldrich) were added. Adding a mixture of 2.5 g $\text{NH}_4\text{S}_2\text{O}_8$ (Merck) and 13 mL 1 M HCl the flask was cooled (0°C). The color of the solution changed from almost white to very dark green. The reaction was stirred overnight, whereas temperature was kept constant between 0 – 4°C. Polymer was filtered and washed with plenty of acetone, water and 1 M HCl. After washing, the solid was dried overnight via freeze-drying (-52°C; 0.062 bar). Afterwards it was milled and pressed to a tablet (20 bar). Manufactured electrodes had a thickness between 1.1 (118 mg) and 0.6 mm (52 mg), which was important for EIS measurements later on.

Polypyrrole

Polypyrrole investigations were executed like published by Carlsson et al.²¹. 320 mg pyrrole (Alfa Aesar) were mixed with 400 mL water and sonicated. Afterwards 100 mL 0.5 M HCl, 60 µl of SPAN 85 and 2 mL pyrrole (distilled) were added and stirred for 5 minutes. 18 g

FeCl₃·6H₂O (Fluka) and 100 mL 0.5 M HCl were prepared and stirred. Both solutions were mixed afterwards and stirred for another 30 minutes. Filtering and washing with 5 liter 0.5 M HCl and 0.1 M NaCl (VWR Chemicals) solution removed all residues.

Increasing the surface area by enzymatic degradation of cellulose

100 mM sodium acetate buffer from Sigma-Aldrich at pH 4.8 was mixed with the enzyme cellulase (5 mg/mL) from trichoderma viride⁴⁹ The mixture was dropped over the composite and stored in an oven at 35°C for 120 minutes to complete turnover of cellulose.

5.5. Electrode preparation

Two different methods were applied for preparing electrodes.

Polymer coated fines were pressed into a pellet of 10 mm diameter with a pressure of 20 kPa for 5 minutes.

Activated carbons were diluted with 1-Methyl-2-pyrrolidinone (abcr) containing between 0 and 20% Kynar 761. Table 7 depicts an overview about all tested compositions. Furthermore, the amount of carbon black was varied to improve conductivity. Before starting with coating, the shiny side of aluminum was fixed on a glass plate. Furthermore, the dull site was cleaned, starting with water, secondly 0.1 M KOH and finally again water. After drying, the slurry was doctor bladed (300 µm) dried on air and later on in an oven at 50°C.

After determining the thickness, electrodes were stamped out and weighed, the circular form had a diameter of 10 mm.

Table 7 Composition of different electrode slurries

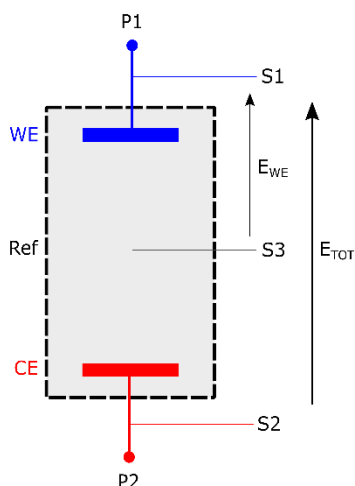
Label	Activated Carbon	Temperature [°C]	Binder [%]	Conducting carbon [%]
MH4	Fines	800	-	
MH6	Fines	800	15.3	
MH8	Fines	950	8.3	
MH9	Fines	950	10.7	10.7
MH11	No fines	-	11.4	8.3
MH15	Fines	800	10	

5.6. Cycling voltammetry and galvanostatic measurements

All electrochemical measurements were performed using a MPG-2 potentiostat (BioLogic) assembling Swagelok®-cells as shown in Fig. 22. Working electrode (WE) and counter electrode (CE) were the same. The reference electrode (RE) partially delithiated LiFePO₄ that has a with a constant voltage of 3.45 V vs. Li/Li⁺.

The cells were assembled in an Ar filled glove box to exclude N₂, air and moisture. Therefore, Swagelok®-cells were assembled inside an argon filled glove box, with an oxygen content < 0.1 ppm and a water content between 0.1 and 0.8 ppm. Both chemicals were transferred into the glove box at the beginning of the measurements and the electrolyte was always freshly mixed inside. The glove box was a UNIlab Plus Glove Box Workstation (MBRAUN).

The cell connection for SC measurements is shown in Fig. 21.



Connection:

- The working electrode (positive) consisted of S1 and P1
- The counter electrode (negative) combined S2 and P2
- S3 is wired to the reference electrode

As usual, the potential was regulated between S1 and S2, E_{we} reached the total potential adjusted before, single electrode potential could be achieved by selecting E_{CE} and $E_{RE} - E_{CE}$.

Figure 21 Wiring of the supercapacitor for all electrochemical measurements

- Showing the progress of the total potential (S1 – S3) between both electrodes
- $E_{we} - E_{ce}$ showed positive electrode potential (S1 – S3) versus reference
- E_{ce} showed negative electrode (S3 – S2) versus reference

Therefore, it was also possible to plot all potentials as a function of time.

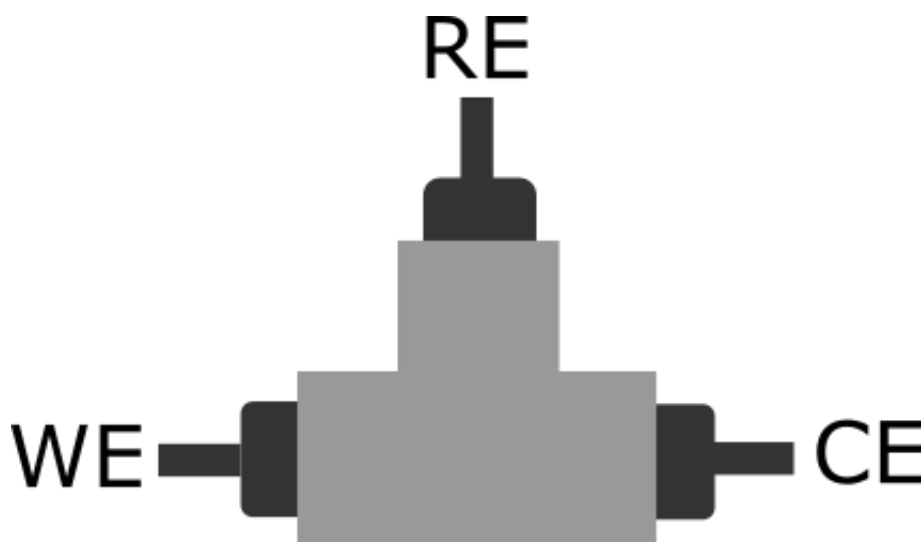


Figure 22 Scheme of the wiring of a Swagelok[®] cell during the electrochemical measurements

In fact, it is important to define a procedure. Otherwise, reproducible results are hardly achieved. Therefore, a schedule was established, the sequence started with the CV followed by galvanostatic measurements.

The setup was listed in table 8 and 9. At the beginning, the current between WE and CE was minimized by a short cut. Furthermore, it was also the starting point for deflections.

Table 8 Cyclic voltammetry settings for testing supercapacitors.

Cyclic voltammetry			
Scan	Scan E_{WE} (dE/dt) [mV/s]	Cycles	Vertex Potential [V]
1	2	4	2.3
2	10	4	2.3
3	20	4	2.3
4	50	4	2.3
5	100	4	2.3
6	200	4	2.3
7	500	4	2.3

Table 9 Galvanostatic settings for testing supercapacitors.

GCPL				
Scan	I_S [mA]	Limit E_{WE}	I_S [mA]	Limit E_{WE}
1	1.5	2.3	-1.5	0
2	3	2.3	-3	0
3	9	2.3	-9	0
4	18	2.3	-18	0
5	36	2.3	-36	0
6	75	2.3	-75	0

7	18	2.3	-18	0
---	----	-----	-----	---

5.7. Self-discharge and leak current

At first, self-discharge measurements took up to 48 hours. First, the voltage was kept constant for 20 minutes at the operating voltage. After this period, the measurement started recording the open circuit voltage. The measurement stopped after reaching half of the operating voltage, which was 1.15 V in this case.

Second, the leak current was measured after charging the supercapacitor and keeping the voltage constant. The current between the electrodes decreases to a plateau, which is used for the calculations.

5.8. Delithiation of LiFePO_4

3.17 mmol LiFePO_4 was stirred with 12.5 mL distilled water to form an aqueous suspension. 200 μL glacial acetic acid (Sigma-Aldrich) and 500 μL hydrogen peroxide (30 % from Roth) were added to 5 mL of distilled water. This solution was added to the suspension and stirred for 2 hours. The suspension was separated by an ultracentrifuge (3500 rpm; 5 minutes). Washing three times and drying at 60°C finalizes the delithiation. For the determination of the degree of delithiation an XRD was taken, a degree of 94% is reached (Fig. 23). The yield of the whole process was 90.8%.

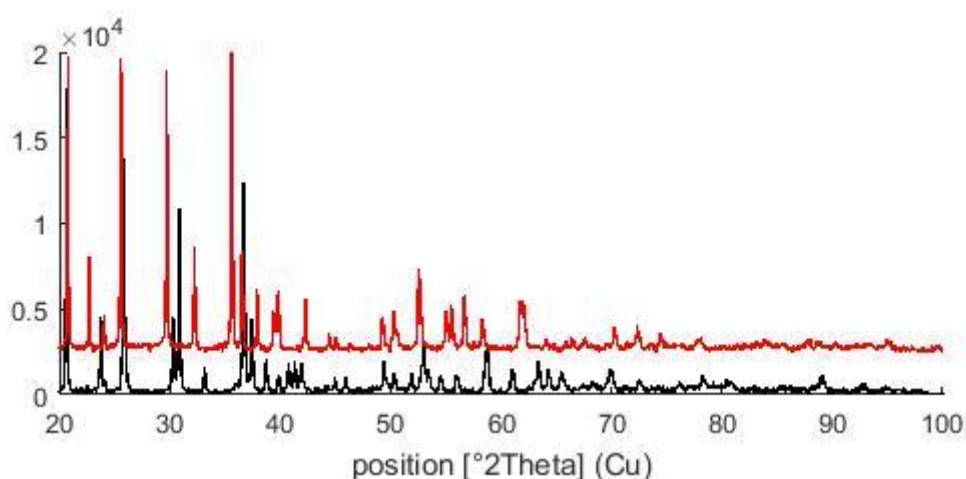


Figure 23: Delithiated LiFePO_4 (black) verified by comparing XRD data with LiFePO_4 (black)

5.9. Chemicals and materials

Table 10 All chemicals applied in experiments

Chemical	Company	Batch number	Purity [%]
Potassiumhydroxide	VWR Chemicals	14K030054	85.0
HCl	VWR Chemicals	16B040516	36.4
Hydrogen peroxide	Roth	206244065	29.0-31.0
NaHCO ₃	VWR Chemicals	14F130017	>99
1-Methyl-2-pyrrolidinone	Abcr	1004974	>99
Aniline	Fluka	1150668	>99.0
Pyrrrol	Alfa Aesar	10127628	>98
Dimethylformamide	Sigma-Aldrich	SZBF340U	>99.8
NH ₄ S ₂ O ₈	Merck	K19701601	>98
Tert.- butanol	Roth	36788929	>99.5
FeCl ₃ ·6H ₂ O	Fluka	371978/1 23097	>99.0
NaCl	VWR Chemicals	14B060025	100
TEABF ₄	Alfa Aesar	61300925	>99.0
Acetonitrile	Sigma-Aldrich	SZB6052AV	>99.9
Sodium acetate	Sigma-Aldrich	SZBD1560V	>99.9
Super P	TIMCAL	-	-
Kynar 761	Arkema	-	-
Reference carbon	Jacoby Carbon Company (PICA)	-	-
Cellulose Nanocrystals	Prepared by acid hydrolysis		

6. Results and Discussion

6.1. Process overview for activated carbons

All process steps except quality control are shown in Fig. 24. First, the paper pulp is diluted and fines are separated from the pulp. The amount of fines is rather low after straining. Therefore, it is necessary to increase the concentration before freeze-drying. Thicker suspensions also save energy in this energy-consuming step. Before grinding with KOH, foam like fines are precarbonized (400°C). The activation was executed at over 800°C in inert atmosphere. Finally, carbonized cellulose is added to form a slurry with the binder before doctor blading. The final form has to be a round 10 mm circuit to test the electrochemical material. The cell was assembled in a glove box and electrochemically characterized.

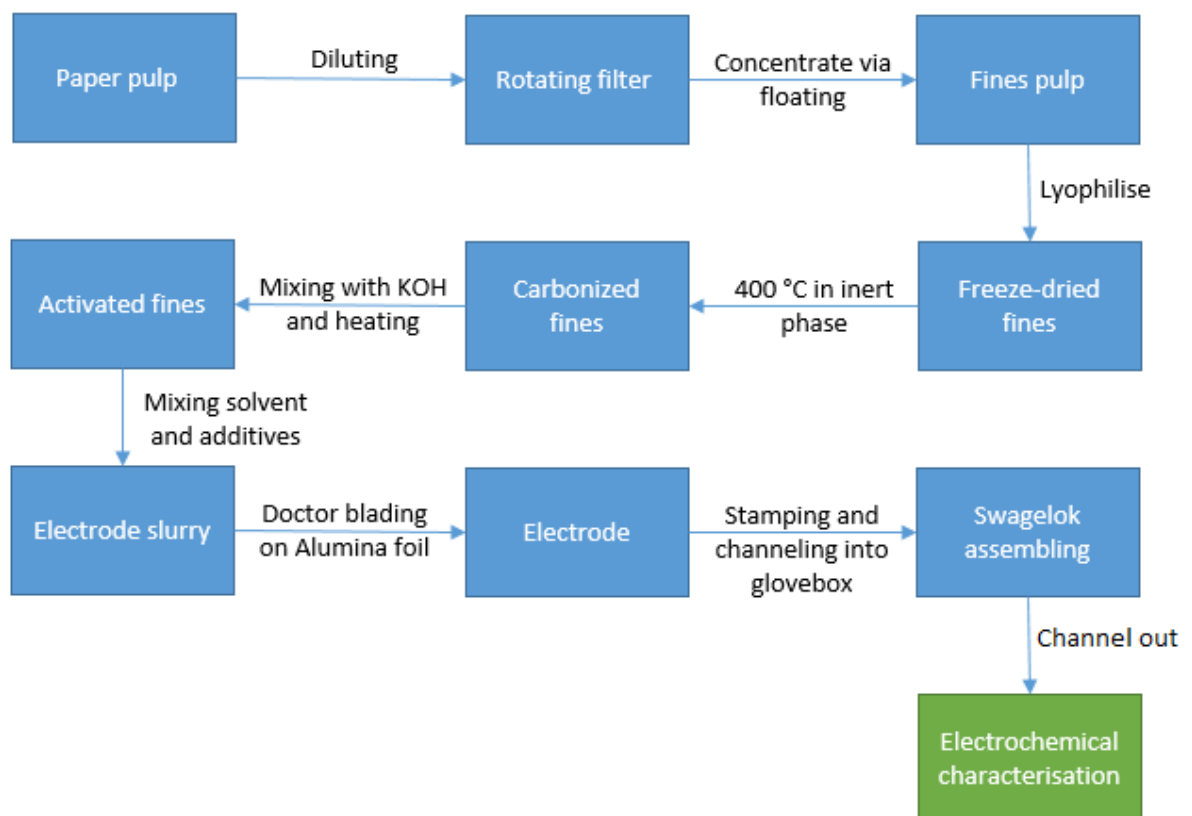


Figure 24 Process overview, from paper pulp to electrochemical characterization of a supercapacitor.

6.2. Elementary trace analysis

In a first step, the purity of the used fines was studied. For this purpose, the fines were subjected to elemental analysis. Since fines originate from the Kraft process, it can be

expected that major amounts of sodium and sulfur were still in the material which has not been subjected to bleaching before use. If there were high amounts of sulfur and sodium in the fines, these would require an intense washing of the materials since these impurities may have a negative impact on the performance of electrochemical storage devices. The results are depicted in Tab. 11. They clearly show that the fines do not contain significant amounts of sodium and very low amounts of sulfur. Therefore, the fines were directly used for the design of energy storing media.

Table 11 ICPMS analysis, of sodium and sulfur content in fines

Sample	S [g/kg]		Na [g/kg]	
	Mw	Std. dev	Mw	Std. dev
Unbleached Kraft pulp	1,4	0.1	0.42	0.04

6.3. Freeze drying of fines

In the next step, the fines were dried. Since drying on air or in the oven causes a change of the fines' supramolecular structure, lyophilization was chosen to remove water from the material. As a consequence, lyophilization retains the porous structure of the highly swollen network which is of utmost importance in the design of electroactive materials.

6.4. Activation processes

In order to increase the surface area it is required to activate the fines. Firstly, these procedures lead to the formation of very small pores, which increases the surface area and the capacity. Secondly, heteroatoms are embedded in the cellulose structure and the electronegativity is improving the capacity.

Comparing different activation processes is an important task to find a proper method to reach the highest surface area and a pore size close to one nm. Surface area was determined by BET analysis. All results of the comprehensive comparison are listed in Tab. 12.

Table 12 BET analysis comparing the differences of the surface area of various activation processes.

Sample	Type	m ² /g	Activation method
1	Primary	12	150°C; Activation in the microwave with aqueous 1 M KOH
2	Primary	973	800°C; Activation by mixing with NaHCO ₃
3	Primary	1521	800°C; Activation by mixing with KOH
4	Primary	974	800°C; Activation without mixing with KOH

5	Primary	5	400°C; without activation
---	---------	---	---------------------------

Sample 1 showed the smallest surface area of all activation processes. It is slightly higher than the surface area, which have been found for non-activated fines. Activation without mixing KOH and pre-carbonized fines (Sample 4), showed very similar results to sample 2 (NaHCO₃ activation). Both are much lower than sample 3. The high amount of publications in recent years gave already evidence that mixing with KOH will result in the highest activated surface area. Thus, KOH mixed with fines are used for all further activation processes. Sample 5 is only precarbonized, which leads to the lowest surface area. The measured surface area corresponds to reported data.³

Of special interest was the difference between primary and secondary fines. The surface area of non-activated secondary fines is reported to be 3 times higher than the surface area of primary fines. Based on the results achieved by BET we chose to proceed with one type of fines. Again a test series was started. Table 13 compares the results between primary and secondary fines. Furthermore, the effect of mixing KOH with fines was investigated.

Table 13 Comparing surface area of activated primary and secondary fines, measured through BET measurements.

Sample	Type	m ² /g	Pore size [nm]	Activation method
4	Primary	1521	2.3	800°C; Activation by mixing with KOH
7	Primary	974	-	800°C; Activation without mixing with KOH
6	Secondary	1370	2.3	800°C; Activation by mixing with KOH
8	Secondary	478	2.6	800°C; Activation without mixing with KOH

In contrary to the expectations, the surface area of primary fines is 10% higher than for secondary ones (Sample 4/6). Non activated secondary fines (10-20 m²/g) exhibit a higher surface area than primary ones (4-5 m²/g). The differences between primary and secondary fines are even larger without mixing and grinding.

Figure 25 shows fines after the different process steps for activation. On the left side the suspension with 4.06 wt% fines is pointed out. The second vial in the middle is filled with freeze-dried fines. Activation is the last step of the process; therefore, the last vessel is filled with activated carbon (right), which is used for electrode preparation.

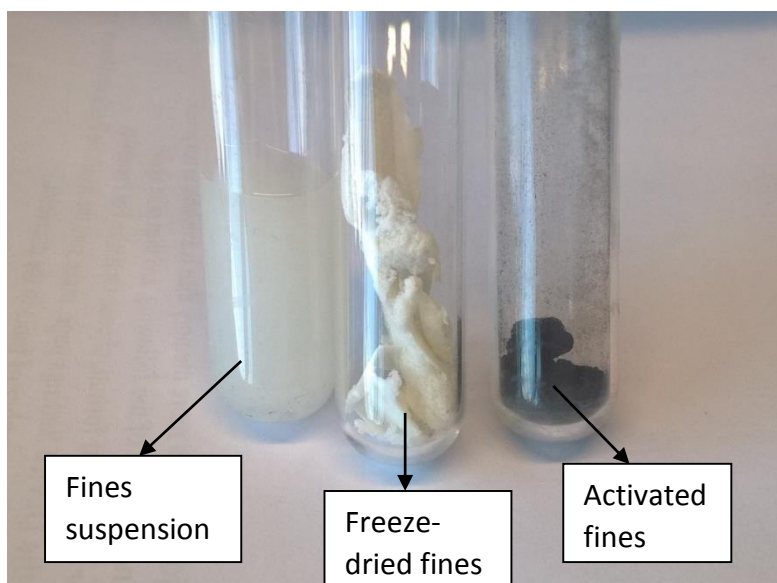


Figure 25 Visualization of fines during all process steps, starting with fines in the suspension, over freeze-dried fines and finishing with activated fines

Surface area has also a big influence on capacities of pseudocapacitors, like for ECDLs. Thus, it is important to adjust the amount of polymer. In syntheses a 20-30 fold surplus of polymer was tested. Still, BET for PPy and PANi coated fines did not show the expected results. In all publications, surface area was between 3 and 30 times higher^{20,19,21}. Synthesizing PANi the reaction vessel was cooled (0°C) during adding the acidic ammonium persulfate solution. Otherwise, chains are getting shorter and conductivity is decreasing. Two further experiments have been executed. First, reports implying the increase of surface area by changing the solvent were found. For example, Carlssons²¹ investigations concentrated on the solvent exchange to *tert*-Butanol. Solvent has to be changed, first through filtration, and then the composite is dissolved in methanol, after filtering again ethanol was used. *Tert*-butanol was the final solvent, while freeze-drying the sample and measuring the surface area again. Second, a further experiment employed cellulase for polypyrrole-coated fines to increase the surface area by caving the polymer. The solvent change as well as the deployment of cellulase did not significantly increase the surface area. Neither this nor the solvent change lead to a sufficient increase of surface area compared to literature. Obviously, cellulose was highly covered; therefore, outcome from the post treatments was rather poor. All measured surface area are summarized in Tab. 14.

Table 14 BET analyzing the differences of the surface area of polymer-coated fines

Sample	Type	Polymer	m ² /g	Additional information
5	Primary	PPy	10.46	

7	Primary	PPy	10.8	Cellulase
6	Primary	PANi	15.2	
8	Primary	PANi	16.9	t-BuOH

Nevertheless, the result should not be overrated, because publications report that distribution of pore size is much more important than the actual surface area.⁵⁰ Also pores below 1 nm have a big influence on the capacity.

6.5. Composites with fines from wood.

As discussed briefly, surface area has a big influence on the performance of the storage material. Wooden composites were mixed with the fine suspension to increase the hierarchical order. Table 15 lists all compositions and results measured with BET.

Table 15 Determination of the surface area of mixed wooden composites.

Suspension	Mass ratio [%]	CNC [g]	Fine [g]	Surface area	Pore size [nm]
1	1:10	3.6	0.4	2169	2.3
2	1:1	2	2	1925	2.2
3	10:1	0.4	3.6	1763	2.4

Through size differences between CNC's and fines it was possible to increase the surface area and minimize the pore size at least for the 1:1 mixture. All other suspensions exhibit higher pore sizes. There are two options why pore sizes do not change while surface area increases. First, CNC's have a similar pore size, or the pore size of CNC's can be neglected because pores are not accessible. Otherwise, it would not be possible to reach higher surface area, keeping constant pore size. This is also interesting to declare for further hierarchical applications.

6.6. SEM analysis

The surface of carbonized fines were investigated without activation. Figure 26 shows the precarbonized cellulose with different magnifications. Poor conductivity inhibits investigations in smaller pores. Nevertheless, this highly porous structure evidences to reach similar results with activation. Best results are achieved by using an InLens detector, otherwise pores were blurred. The pore size is determined on (b) and was 130 nm.

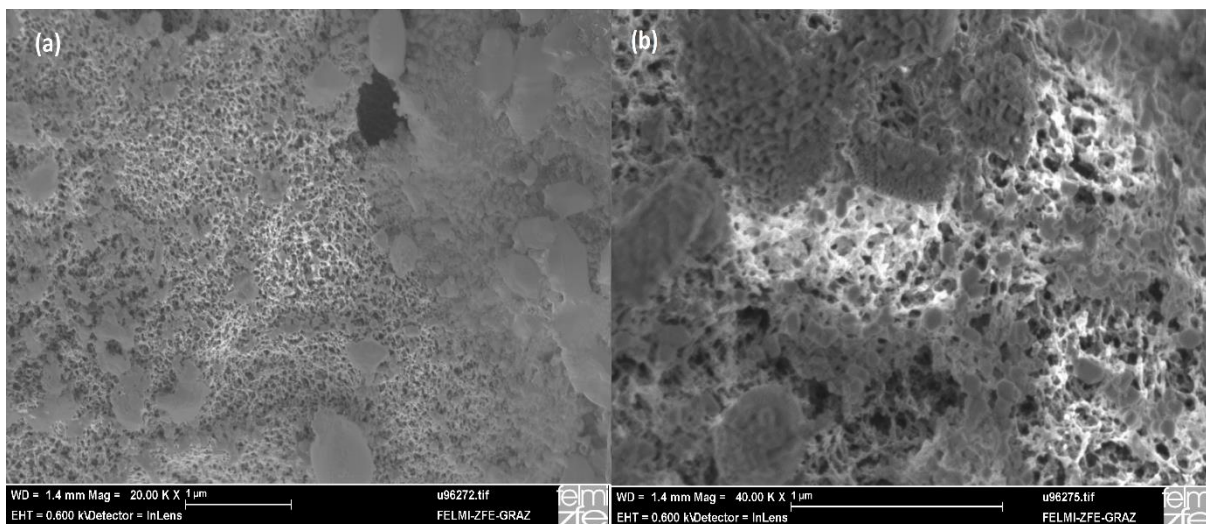


Figure 26 SEM images of precarbonized cellulose, showing the highly porous structure with different magnifications ((a) 2000 fold and (b) 4000 fold).

Afterwards, investigations concentrated on KOH activated (800°C) fines. In average particle sizes between 20 - 50 μm have been detected in SEM (Fig. 27 (a)). Particle size also determines film thickness for electrodes. The same settings (Fig. 27 (b)) did not show any pores on the surface. Further magnification gave a clue if pore size decreased due to heat.

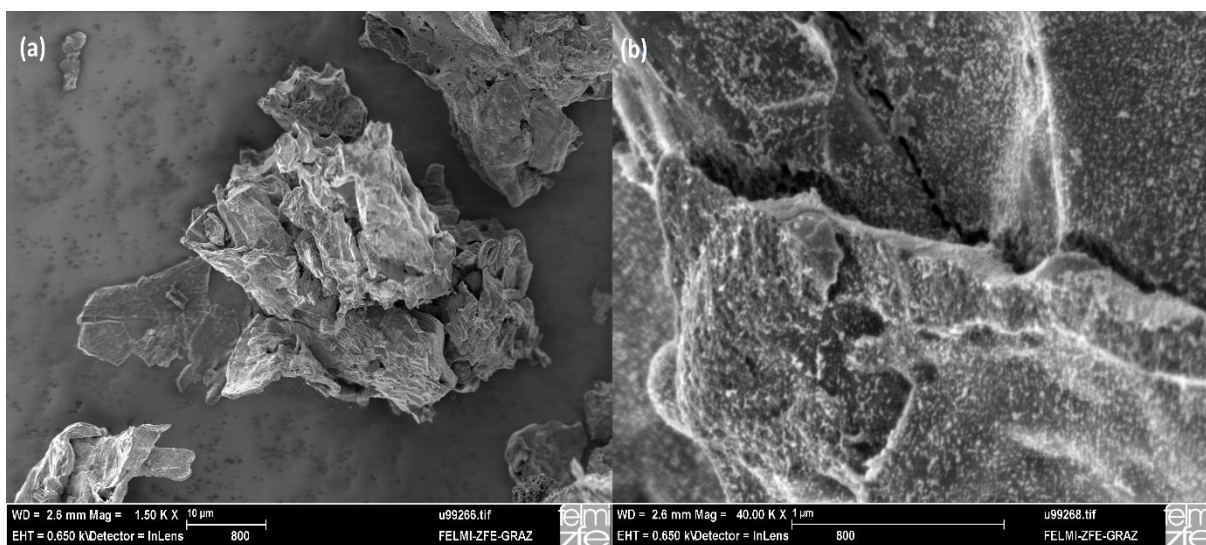


Figure 27 SEM pictures A) shows the average particle size. B) the main surface, no porosity can be observed, but a net like structure on a view corners, which is highly porous.

Figure 28 exhibits that pores did not vanish, they were decreasing down to half of the size measured at Fig. 26. Results achieved through BET measurements already confirmed the acceptance of a highly connected pore system inside the 50 μm particles, which is desirable for the attachment of ions on the surface.

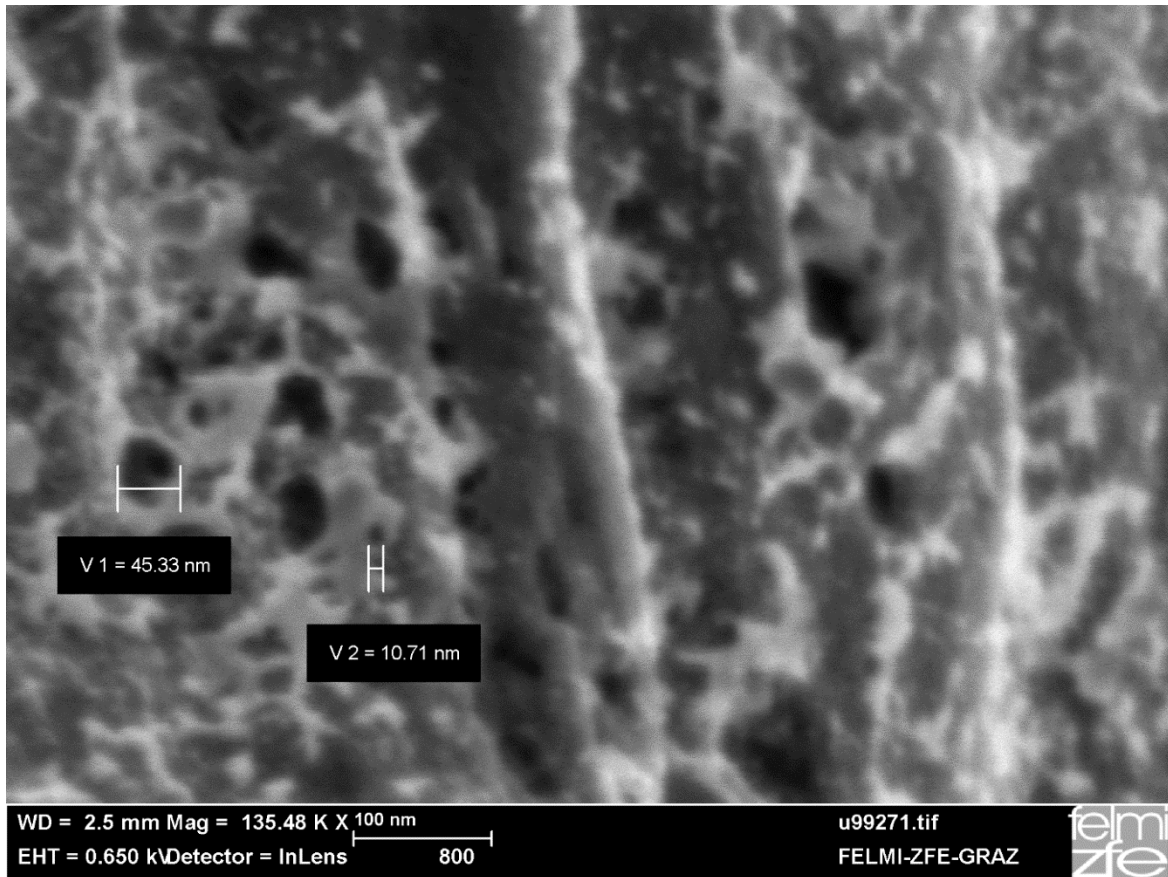


Figure 28 SEM picture investigating in the pore size of AC, activated at 800°C.

6.7. Infrared Analysis (IR)

In a first step, IR spectroscopy was used to monitor activation progress. The number of functional groups on cellulose was directly relating to the degree of carbonization. Functional groups reacted to gases and were blown out with the inert gas stream. In course of the precarbonization of the activation process, functional groups were reduced (Fig. 27). A further minimization of functional groups was obtained during carbonization. At the end, the former cellulose was heated to 800°C. Figure 29 illustrates the process, which ends with elemental carbon. Therefore, the carbonization process was successful. All solid residues have been measured on the ATR-IR spectroscope.

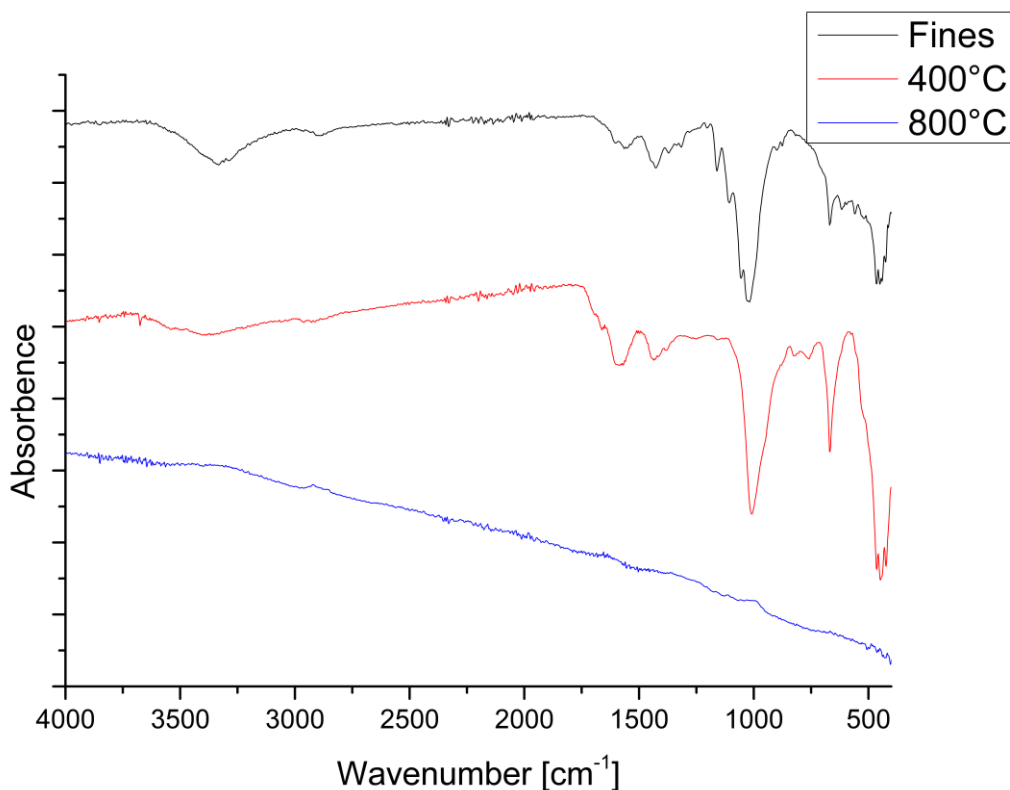


Figure 29 IR data exhibiting the decrease of functional groups during the activation process, depending on temperature.

6.8. Investigations of the purity of activated carbon

Ions interfere in electrochemical reactions, thus activated carbon was washed three times with distilled water and separated by centrifugation. Traces from elements like sulfur or sodium in carbon may have a big impact on cycle stability during the charge/discharge process. Therefore, the purity was investigated by EDX (Tab. 16).

Table 16 Trace analysis by EDX to determine impurities in activated carbons.

Element	800 °C		900°C	
	Weight ratio [%]	Std. deviation [%]	Weight ratio [%]	Std. deviation [%]
C	72.1	1.24	58.8	3.74
O	22.5	1.83	26.9	0.92
Si	4.62	2.67	11.1	3.68
S	0.76	0.31	0.68	0.21
Cl	-	-	0.525	0.015
K	-	-	2.03	0.765

The activated carbon contained rather small amounts of elemental traces (Si, S, Cl, K) which should not influence the performance. The high amount of silicon is based upon scratching in the ceramic reaction vessel before stirring in HCl solution. The carbon, which was activated at 900°C, showed much higher amounts of potassium because of the washing step. Anyway, the amount of potassium measured in the carbon is not significant. Furthermore, it did not reveal a direct influence on the adsorption process.

6.9. Electrode manufacturing

In comparison to polymer-coated carbon the activated carbon is rather brittle. For this purpose, a support material is needed for mechanical stabilization. The carrier material is directly connected with the pistons of the Swagelok® cell, for this reason conductivity has to be much higher compared carbon. Otherwise, the serial resistance becomes the performance limiting parameter. Furthermore, the carrier materials has to be inert in the cell environment and the potential scale. Therefore, activated carbon was doctor bladed on aluminum. Irregularities on the aluminum directly affects the electrochemical properties of the electrode. The slurry was a mixture of AC with PVdF binder and N-methylpyrrolidone (NMP) as solvent. Additionally, different compositions of binder and conductive carbon were tested to improve the electrode properties.

The electrodes were punched to a size of 10 mm (Fig. 30) and dried at 120°C under vacuum (10^{-2} bar) for at least 2 hours. Afterwards, the electrodes were transferred to the glove box. Ambient humidity would reduce the applicable potential window of the electrolyte due to H₂ and O₂ evolution. This effect can be avoided by assembling the cell in a glove box, whereas cells applying aqueous electrolytes can be assembled in air.



Figure 30 Fabrication of the electrode (10 mm) by stamping the doctor bladed, activated cellulose on the aluminum carrier.

6.10. Electrochemical analysis

In order to achieve the best results, different parameters were tested. Firstly, the slurry was varied to achieve stable and highly conductive electrodes. Since ideal electrodes are not limited by conductivity, the resistivities of the activated materials were measured and compared with each other.

The first slurry was AC activated at 800°C without binder (MH4), testing adhesion between carbon and the aluminum surface. Secondly, the sample MH6 used carbon activated at 950°C and 15 % binder to avoid problems with adhesion. Further comparisons were made between carbon activated at 950°C with less amount of binder (MH8) and by adding non activated carbon (Super P) to improve conductivity of the whole electrode. Pollak investigated the change of conductivity by polarization if the pore size is sufficiently large.⁵¹ In order to prevent lower conductivity conductive carbon was added to the suspension.

Beside MH11 all electrodes were made from fines. MH11 was a reference carbon, namely PICA from Jacoby Carbon Company, it was used to compare the electrodes manufactured out of fines with an established electrode material.

Further investigations with different activation temperatures were obtained by comparing the BET surface areas as a first indication. The electrochemical performance is, however, the ultimate goal and was tested in Swagelok® cells.

6.10.1. EIS of EDLCs electrodes

The thickness of the dry layer of the activated carbon was always depending on the amount of binder and particle size, which was determined to be between 20-50 μm (Mitutoyo ID-F125). Averaging the thickness of three samples from the same electrode conductivity can be calculated from the measured impedance (Tab. 17).

The EIS measurements were carried out over a frequency range of 1 MHz to 100 mHz. Slight variations in the measurements of the same sample can be ascribed to varying contact resistance. Different particle sizes roughen the surface and increase the contact resistance. For this reason, the measured resistance is higher than reported in literature.

Table 17 Impedance data of the activated carbon electrodes, varying slurry compositions.

Sample	Temperature [°C]	Binder [%]	Avg. thickness [cm]	Resistance [Ω]	Conductivity [mS/cm]
MH4	800	-	0,0053	7	0.966
MH6	800	15.3	0,00175	30	0.0746
MH8	950	8.3	0,00555	1,3	5.44

Particle size was estimated to be in the range of 20 - 50 μm as seen in SEM images. This also influences thickness and explains thickness variations of electrodes using the same activated carbon source.

6.10.2. EIS of pseudocapacitor electrodes

Fines from wood coated with conductive polymers are limited to aqueous electrolytes. Recently reported conductivities range from 5 to 500 S/cm². Measured data from coated fines are three powers lower than published (Tab. 18 and 19). Rough surface area limits the contact between the electrode and the stamps. Hence, contact resistance is increased yielding in lower conductivities. The surface can be coated with metals. Smooth surfaces reduce this effect, like gold sputtering for example, which is applied for this reason (Tab. 19).

Table 18 Impedance results for PANi tablets, measured by EIS.

Thickness [cm]	Impedance [Ω]	Conductivity [mS/cm ²]
0.0525	6.3	11
0.0981	98	1.3

0.0912	48	2.4
--------	----	-----

Table 19 Impedance results for PPy tablets, measured by EIS.

Thickness [cm]	Impedance [Ω]	Conductivity [mS/cm^2]	Comment
0.0548	6.8	10	
0.0939	9.0	13	
0.101	5.3	24	Sputtered with gold

Gold sputtering reduces the contact resistance. However, all measured conductivities are still rather low compared to the reported ones.

6.10.3. Supercapacitors with organic electrolytes

6.10.3.1. Galvanostatic measurements

Capacities and efficiencies are the most important factors of supercapacitors. Both parameters can be calculated from the voltage, measured with a controlled current during charging. Typical plotting for potentiostatic measurements are depicted in Fig. 31. The voltage grows nearly linearly with time as expected for near ideal capacitors. Furthermore, these measurements also enable to compare the influence of conductive carbon (Super P) and binder (Kynar 761) on cycle life and capacitances. Due to adhesion problems, the electrodes without binder (MH4) have not been measured potentiostatically. By the use of a binder, the carbon adheres to the aluminum, otherwise stamping is not possible. All further electrodes were measured and shown in Fig. 32. A decrease of the capacity is related to higher fixed currents and faster charging/discharging processes. Faster processes are always accompanied by a worse use of space. This can be observed every fourth cycle.

Further information is derived by comparing electrode materials. In conclusion, activated fines show similar results than the reference carbon, only the capacity is slightly lower. Furthermore, as already expected through BET measurements, a higher activation temperature closes pores and makes them less accessible. Comparing capacities, MH6 electrodes reach even higher capacities than the reference. Additionally, efficiencies are reproducible for all electrodes. While the first cycle shows some variations, the supercapacitor is highly stable when all balances are adjusted. Carbon from MH8 (b) and MH9 (c) were treated

equally and only differ in composition. MH9 contains Super P as additive to improve conductivity. Both of them attain very similar capacities; it can be assumed that an increase of conductivity is not as important as expected.

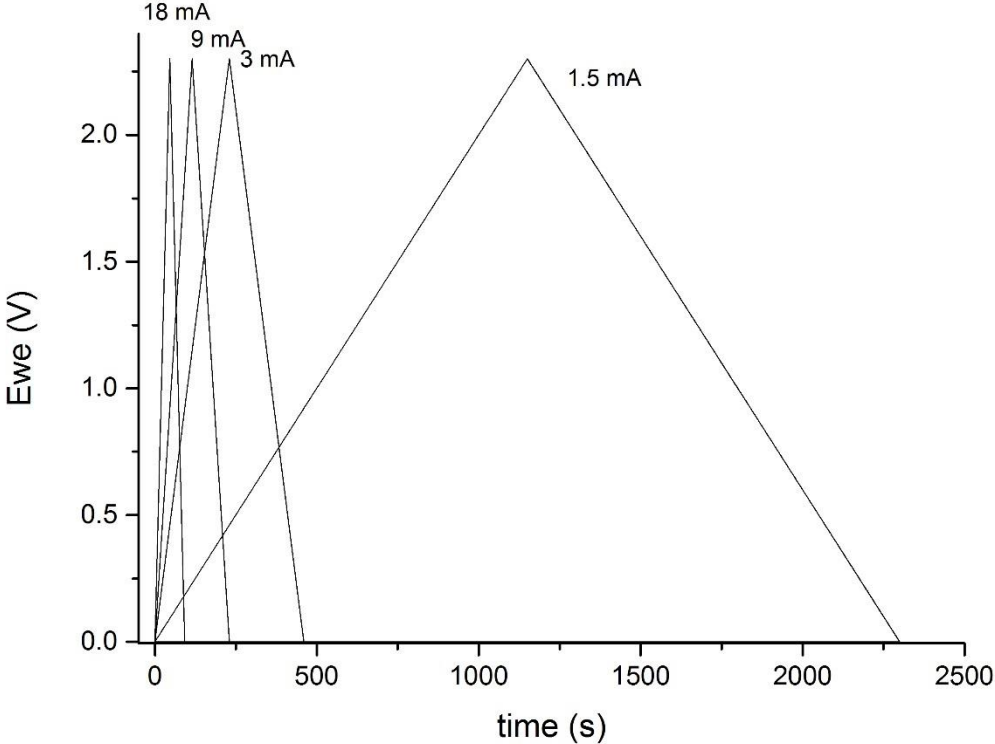


Figure 31 Evolution of the cell potential versus time during galvanostatic cycling at varying rates as indicated in the graph. Rates are absolute currents.

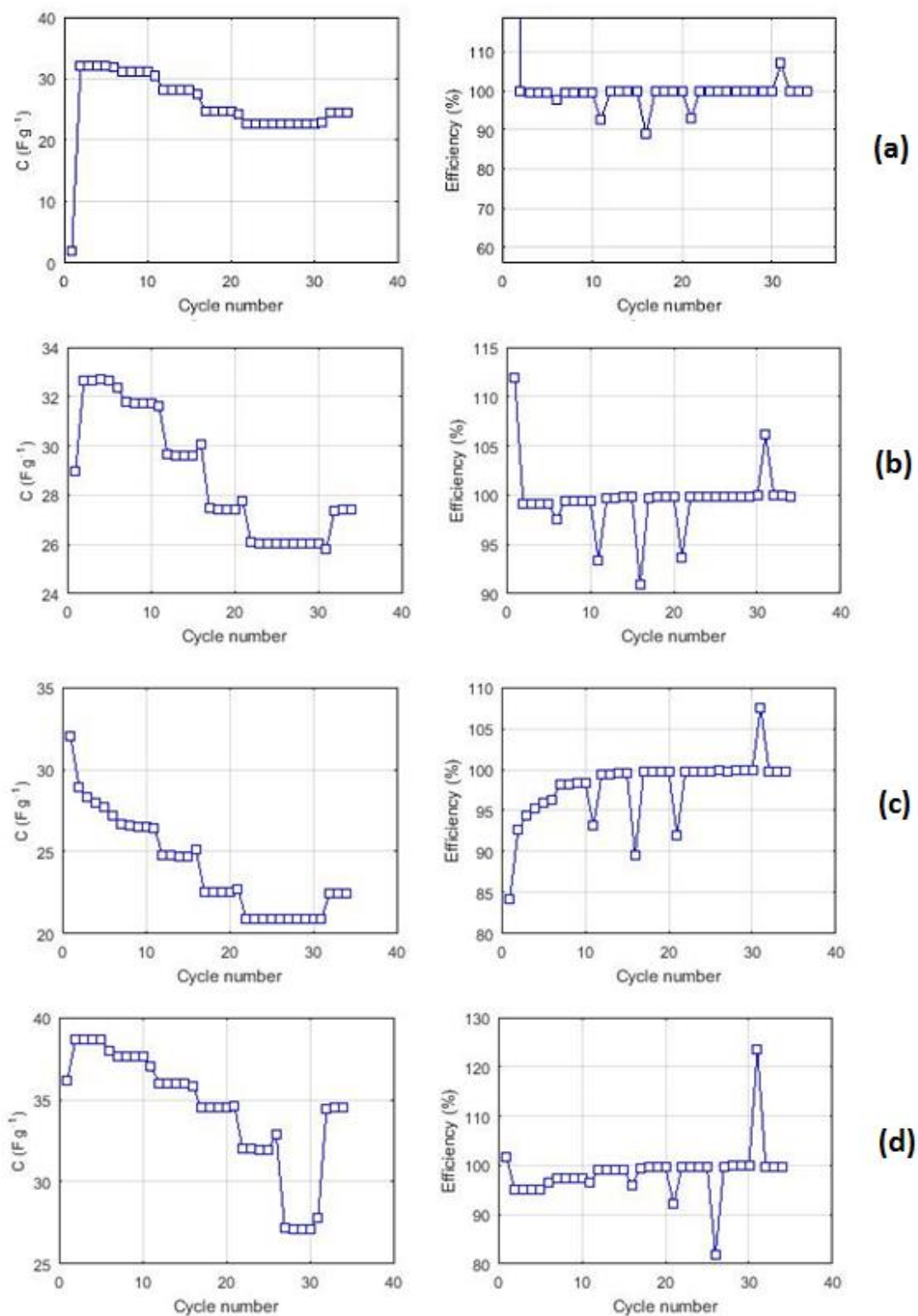


Figure 32 Galvanostatic cycling of symmetric SCs between 0 and 2.3 V at 1.5, 3, 9, 18, 36, 75 and 18 mA for 5 cycles each. The left column shows the specific capacitance and the right column the coulombic efficiency. The electrode material activated at 800°C (a) exhibits higher capacities due to smaller pore sizes. (b) has a similar composition but the carbon was activated at 950°C. The influence of conductive carbon content was investigated in (c). It contained 10% of conductive carbon, leading to more capacity fading as also reflected in lower initial efficiencies. All results were compared to (d) using an established electrode material, namely PICA (Jacoby Carbon Company).

6.10.3.2. Cyclic voltammetry

Best results have been achieved by using electrode material activated at 800°C containing about 15% binder, therefore cyclic voltammetry measurements were performed with them. Figure 33 shows a nearly rectangular shape during the charge/discharge process. A small peak can be observed during the oxidation, in most of the time it is related to decomposition, due to different loadings on the electrodes. Faster scan rates cause a reduction of capacitance (Fig. 34), improper EDLs might be the reason. This process is reversible, which can be observed by decreasing and increasing the scan rate leading to similar CVs.

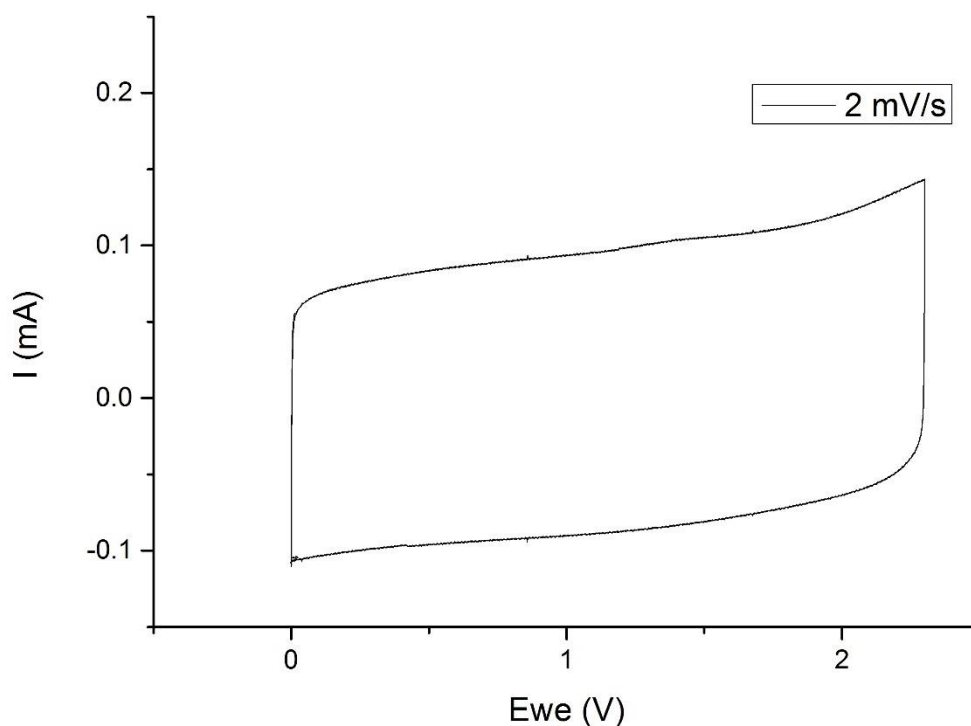


Figure 33 Single CV cycle for an electrode material activated at 800°C containing about 15% binder recorded at a scan rate of 2 mV/s between 0 and 2.3 V.

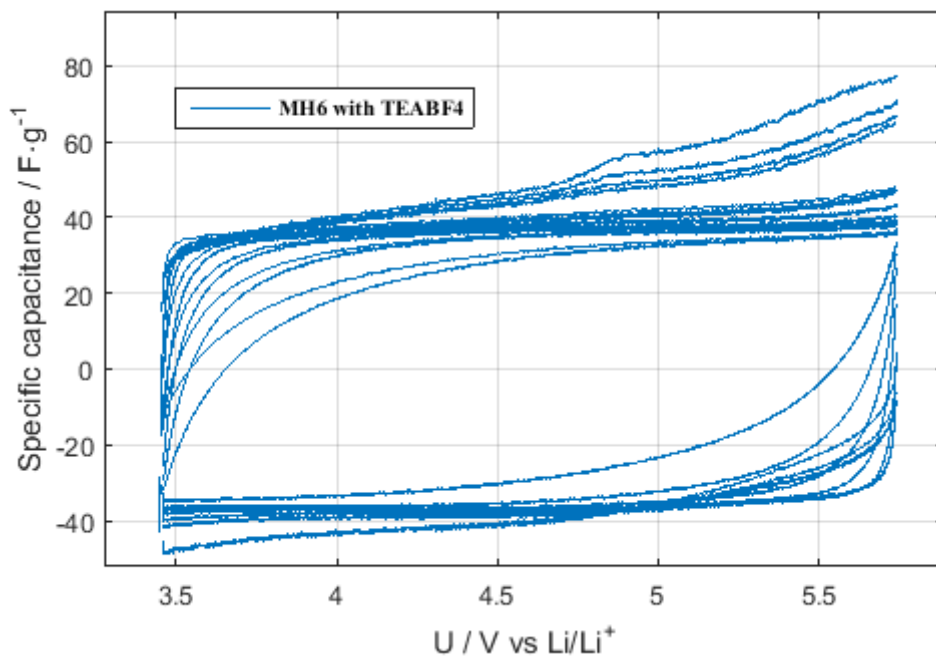


Figure 34 Testing electrode material activated at 800°C containing about 15% binder with organic electrolyte over 36 cycles, plotting specific capacitance calculated out of CV data in dependency of the voltage.

6.10.3.3. Leak current

The leak current is referred to capacity and the potential ($[mA \cdot V^{-1} \cdot F^{-1}]$). The highest current peak is obtained during charging. Afterwards self-discharge starts immediately in form of a reformation of the ions. The decreasing current in Fig. 35 is illustrating this process. Electrode material used for these measurements was activated at $800^{\circ}C$ and contained about 15% binder. After this, the current only needs few seconds to decrease down to 0.05 mA. After 6000 seconds, the current was down to 0.025 mA, this was the value taken to calculate the leak current ($0.18 mA \cdot V^{-1} \cdot F^{-1}$).

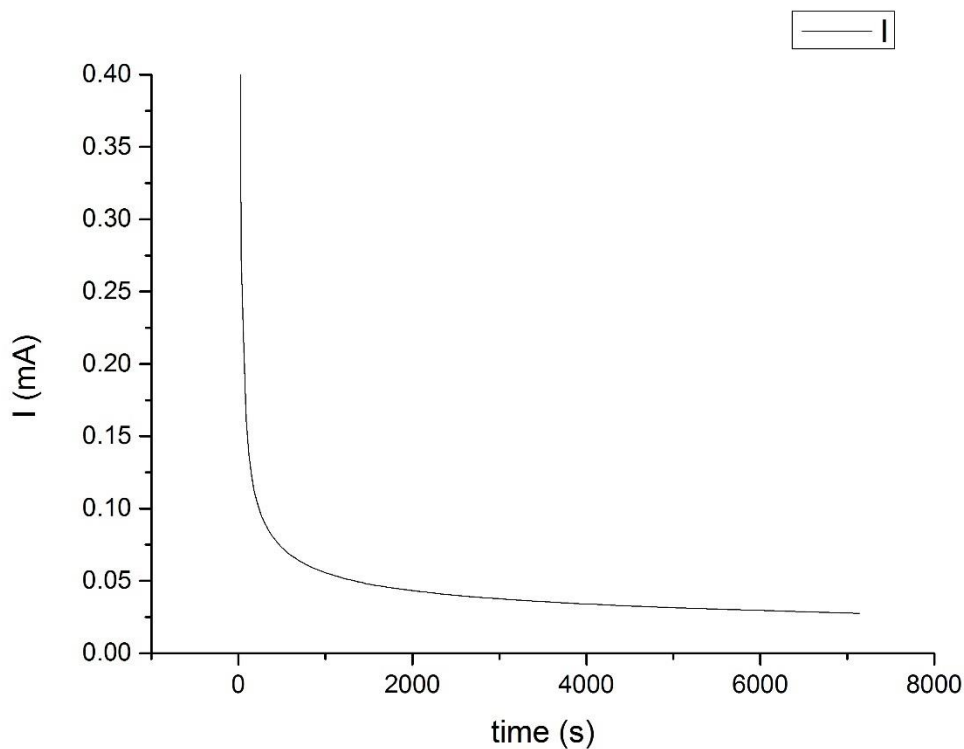


Figure 35 Leak current diagram, after two hours the electrodes activated at $800^{\circ}C$ containing 15% binder reached the plateau of a constant current.

6.10.3.4. Self discharge

Self discharge is illustrated in Fig. 36 of electrodes containing activated carbon (800°) and about 15% binder. It can be seen that 325.5 minutes, or 19 530 seconds are needed to reach half of the operating voltage. Eq. 10 was used calculate the discharge current for the process, resulting in a current of 2.37 μ A.

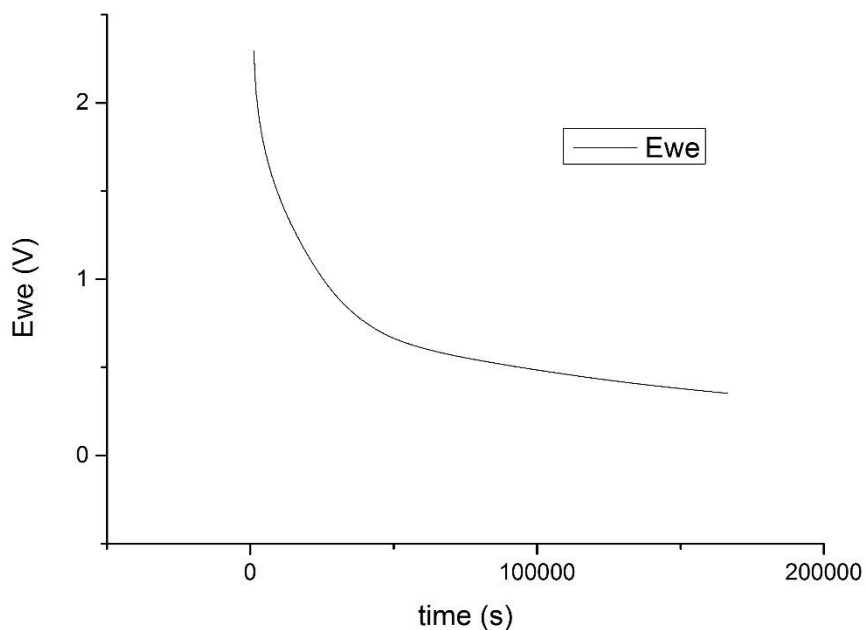


Figure 36 The self discharge diagram of electrodes manufactured like MH6 (Activated at 800°C; 15% binder) The supercapacitor needed 325.5 minutes to be semi-charged.

Comparing self discharge and leak current with an other publication⁵², calculated currents are rather large, thereby faster discharges can be observed.

6.10.4. Supercapacitors with aqueous electrolytes

6.10.4.1. Potentiostatic measurements

Potentiostatic measurements for both electrolytic systems showed decreasing capacities with every cycle (Fig.37). H₂SO₄ as electrolyte results in higher capacities, but at the second cycle, capacity was almost down to zero. As a consequence of the break down, the efficiency is stabilized. At the beginning using KOH as electrolyte, capacity is higher compared to organic media. Comparing KOH and H₂SO₄ the same effect could be observed for H₂SO₄, at a slower rate. Efficiency was stable after the 10th cycle when capacity was down to 20 F/g. Further CV

measurements have been made to compare results with galvanostatic measurements and discuss the outcome.

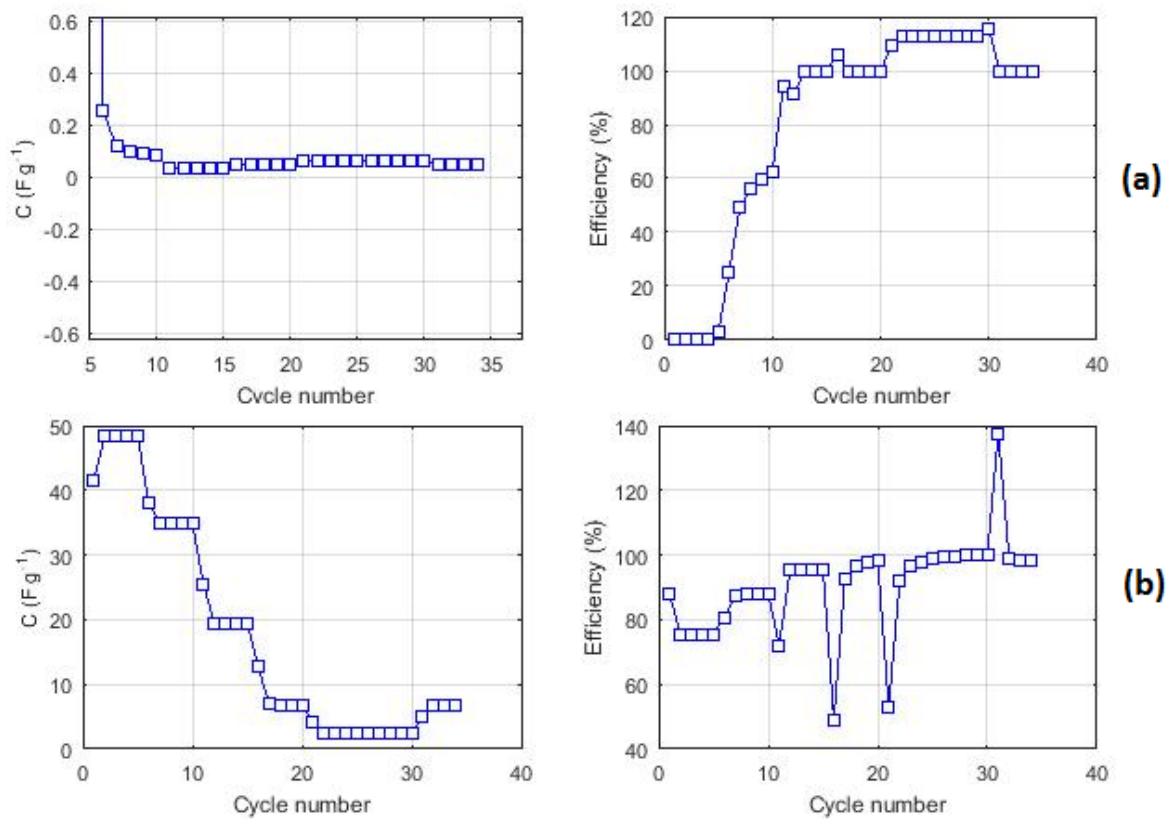


Figure 37 Galvanostatic measurements with aqueous electrolytes, comparing capacities and coulombic efficiency for activated carbons (800°C) containing about 15% binder. Comparing the electrolytes (a) 1 M H₂SO₄ with (b) 6 M KOH.

6.10.4.2. Cyclic voltammetry

Cyclic voltammetry measurements have been used for both systems. The electrodes from MH6 (activated at 800°C, 15% binder) are used for comparing aqueous and organic systems with CVs and galvanostatic measurements. Therefore, 28 cycles with different scan rates have been executed. The capacity decrease is visualized in Fig. 38. Overall, measured capacities close to 300 F/g are promising, but after a few cycles a breakdown is observed. Moreover, longer storage periods of the assembled supercapacitor also reduce the capacity. The same results have been noted in galvanostatic measurements.

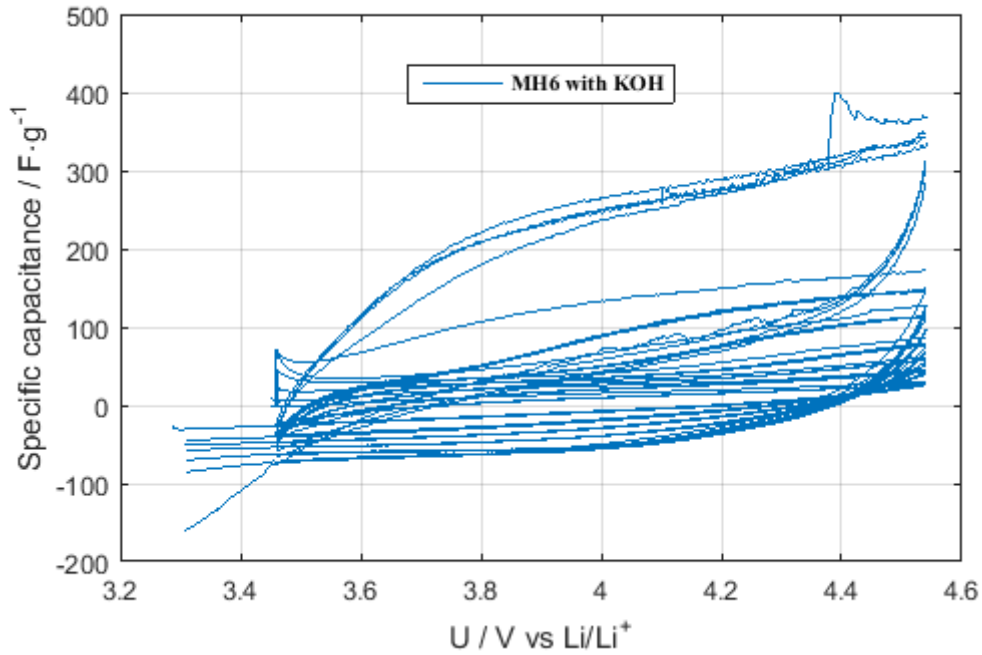


Figure 38 Galvanostatic measurements of the MH6 electrodes with KOH as electrolyte. Plotting the specific capacitance compared to the voltage.

Figure 38 visualizes the decrease of capacity over time. Irreversible reactions result in worse cycling stability of the supercapacitor. As it can be seen on Fig. 39, the aluminum reacts with the aqueous electrolytes. The exothermic reactions inside also restrict the performance of the electrodes. 1 M sulfuric acid reacts with almost all aluminum, only the separator stays inert. On the aluminum surface AC with a salt-like coating is left. In addition, 6 M Potassium hydroxide reacts with aluminum, which takes longer, resulting in a steady decrease of capacity. In literature aluminum is replaced by Nickel foam for measurements with aqueous electrolytes.^{53,54}



Figure 39 Images of electrodes after electrochemical characterization. (a) is with an alkaline as electrolyte (KOH), whereas (b) is measured with H_2SO_4 .

6.10.5. Comparing organic and aqueous electrolytes

Although supercapacitors applying aqueous electrolytes show rather high capacities, their coulombic efficiency is limited with aluminum as a carrier (Fig. 39). The charge and discharge cycles with $TEABF_4/ACN$ and 6 M KOH are compared in Fig. 40. The comparison shows that much more energy is provided for the aqueous system than can be reclaimed out of it. As a conclusion, ongoing reactions in the cell have to be exothermic. Furthermore, CV traces the degradation of the electrodes. The capacities have been compared in the same plot, offering the advantage of organic electrolytes. First of all, the high cycling stability compared to aqueous media is pointed out. Secondly, the potential window can be more than doubled with organic in comparison to aqueous electrolyte. Eventually, Fig. 41 (b) shows promising efficiencies although, after a specific amount of cycles results are getting insignificant due to high losses during the first cycles. In future applications inert carrier materials will be applied to improve cycling stability of aqueous electrolytes.

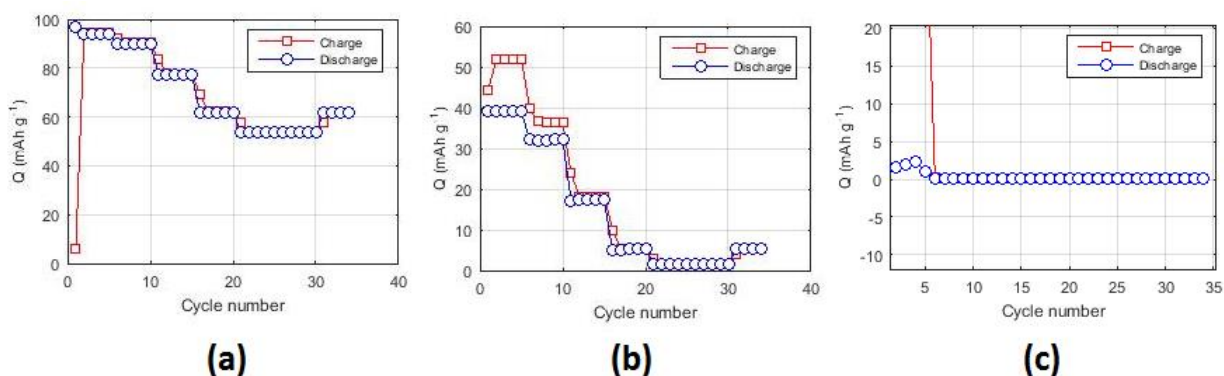


Figure 40 The electrode material was activated at 800°C containing 15% binder. Comparing galvanostatic charge/discharge cycles for organic and aqueous electrolytes. a) TEABF₄/ACN as electrolyte showed highly reproducible cycles. (b) used 6 M KOH as electrolyte losing consequently energy between charge and discharge, 1 M H₂SO₄ was assembled in (c), a high amount of energy is put into the system without any reasonable output.

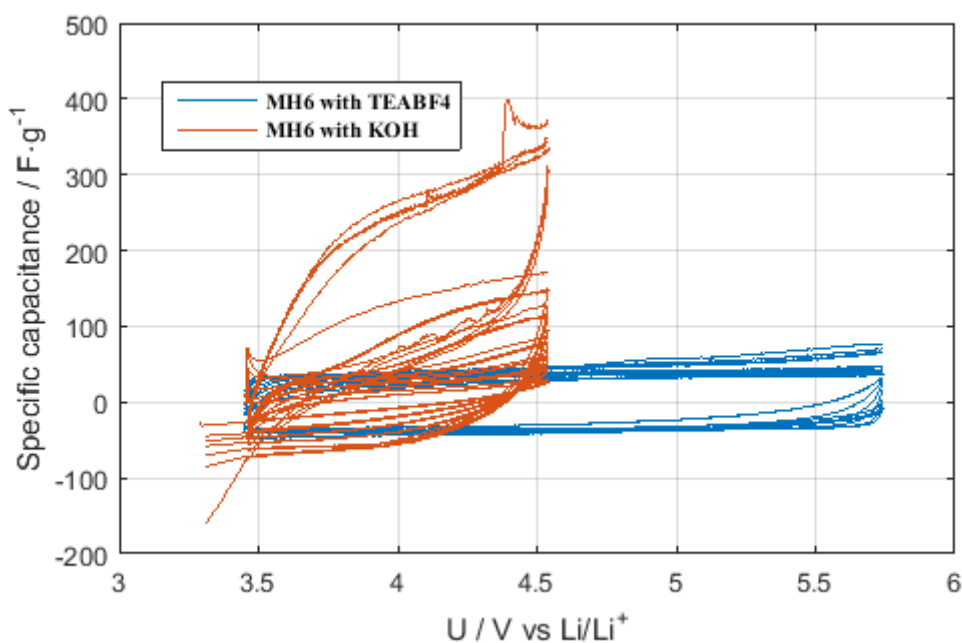


Figure 41 Comparing CV data of supercapacitors using KOH and TEABF₄/ACN as electrolyte (Electrodes containing AC activated at 800°C with 15% binder).

The fast decrease of capacity in aqueous media and the low cycle life are reasons for concentrating on organic media. The results gained from measuring with this system have been highly reproducible and promising for future applications.

7. Conclusion and Outlook

To conclude, we produced supercapacitor electrode materials from a highly abundant side stream material in paper industry. Once more considering all process steps, we started with paper pulp, separating fines from fibers and concentrating the amount of fines in the suspension applying flotation. From that point, we took the properties of the different types of fines into account. Freeze-drying is a very important step to retain the supramolecular structure. First variations have been detected by testing different activation processes. BET measurements revealed that KOH activation emerges as the most promising route. Specific surface areas of 1521 m²/g and a pore size distribution centering around with 2.3 nm were obtained by activating precarbonized fines with KOH.

Alternatively, fines were coated with PPy and PANi, which are conducting polymers, to obtain supercapacitor electrode materials. Initial BET surface areas were rather low in comparison to data reported in the literature on similar systems. As a result of the small surface area we did not assemble SCs with electrodes made from coated fines.

Tests in supercapacitors have shown that high fractions of activated carbon are required for sufficient conductivities. Investigating in organic as well as in aqueous electrolytes enable to compare both systems with each other. The used cell setup did, however, nor allow for reliable measurements with aqueous electrolytes. Therefore, the main focus was on SCs with organic electrolytes. The results for the supercapacitor using organic electrolyte are more promising, capacitances of up to 33 F/g were reached. Highest reported capacities in an organic system are 236 F/g and 100 F/cm² ⁴⁶ per electrode, but this application may pave the way for new ideas in bio-based research.

7.1. Future Outlook

Upscaling the separation of fines from paper pulp would be easily possible for paper plants. Therefore, applications for fines beyond thermal use are very interesting. Energy storage media are only one possibility to apply fines. In the future, we plan investigations in cellulose composites, especially for supercapacitors. The considerable enlargement of surface area by mixing with CNC's enhanced the interest on composites. Further alternatives would be packing materials and filters. Comparing the surface area with similar products like nanofibrillated cellulose (NFC) or even smaller cellulose nanocrystals (CNC). It is obvious that fines have a much smaller surface area than NFC and CNC, due to their particle size. However, fines are a very promising and cheap alternative compared to them. In contrast, all other products have to be produced, fines can be easily filtered. Fines are even more interesting since not all properties have been clarified yet. Novel applications for paper fibers including fines could be easily possible. Every application made out of side streams like lignin or fines saves energy and decreases production costs.

Therefore, fines will be one of the dominant research topics for the paper industry for years to come.

8. Attachments

8.1. Figures

Figure 1 Basic molecular structure of unbranched cellulose, consisting of β -D-Glucose connected via β -1,4 glycosidic bond.....	1
Figure 2 Simplified view on the molecular structure of lignin (left) and xylose (right), one of the most common pentose's in wood.....	2
Figure 3 Unbeaten pulp of spruce (a) and birch (b) compared to thermomechanical pulp (c). The bar on the bottom is 400 μm . ³	3
Figure 4 Fiber structure of a wooden fiber illustrating inner fiber layers ³	5
Figure 5 Image of an optical micrograph from primary (a) and secondary fines (b).	6
Figure 6 Primary fines from wood analyzed by the Malvern Mastersizer 2000, plotting a bimodal particle size distribution versus vol%. ⁶	9
Figure 7 Illustration of a supercapacitor A) Is aluminum to stabilize the electrode material B) the highly porous electrode material, where pores are filled with C) the electron conducting electrolyte. D) Membrane to avoid contact between both electrodes, which will lead to a short cut of the supercapacitor. Below the capacitor is the equivalent electrical circuit of the supercapacitor, which are two serially connected capacitors.....	13
Figure 8 Scheme of an EDL storage illustrating the formation of a double layer. ¹³	14
Figure 9 Overview of supercapacitor types classified by storage mechanisms	16
Figure 10 (A to D) Illustrates different storage mechanism in SCs. (A) shows the electrostatic storage at carbon particles and (B) in pores. Pseudocapacitive energy storage via inorganic materials is exhibited in (C) (e.g. RuO_2). (D) stores energy by intercalating Li^+ . (E-H) compares supercapacitors with batteries. The linear potential change in (E) is typical for all SCs, while batteries show peaks of redox processes (F). The approach of batteries to SCs is depicted in (H) by using nanoscale battery materials. ¹⁷	17
Figure 11 A fundamental scheme of the polymerization of aniline, which reacts to polyaniline.....	20
Figure 12 Reaction scheme to synthesize the green emeraldine salt (conductive state) starting with polyaniline	21
Figure 13 Polymerization of polypyrrole via anodic oxidation.....	21
Figure 14 Doped polypyrrole, which results in higher conductivities.	22
Figure 15 Ragone plot compares different energy storage systems with each other due to specific power to specific energy. ³⁹	23
Figure 16 Cyclic voltammetry signals. (a) Image of a CV, current is almost rectangular, means voltage independency. ⁴⁰	25
Figure 17 Typical galvanostatic measurement illustrates dependency between current rate, voltage and time for charging ⁴¹	27
Figure 18 Randels circuit is an equivalent electrical circuit, used for EIS measurements	28
Figure 19 Impedance measurements of pseudocapacitors with the typical loop at higher frequencies ⁴²	28
Figure 20 Equipment to separate fines from the pulp. (a) shows the whole process starting by pumping diluted pulp out of the ton into the pressure screen, where fines get separated. (b) is an overview of the pressure screen with one inlet and two outlets. (c) is an inner view of the pressure screen, rotor blades are turning a pressing pulp against the perforated strainer, so fines can be separated. Copyright Wolfgang J. Fischer (TU Graz).....	34
Figure 21 Wiring of the supercapacitor for all electrochemical measurements.....	38

Figure 22 Scheme of the wiring of a Swagelok® cell during the electrochemical measurements.....	39
Figure 23: Delithiated LiFePO ₄ (black) verified by comparing XRD data with LiFePO ₄ (black).....	40
Figure 24 Process overview, from paper pulp to electrochemical characterization of a supercapacitor.	42
Figure 25 Visualization of fines during all process steps, starting with fines in the suspension, over freeze-dried fines and finishing with activated fines	45
Figure 26 SEM images of precarbonized cellulose, showing the highly porous structure with different magnifications ((a) 2000 fold and (b) 4000 fold).....	47
Figure 27 SEM pictures A) shows the average particle size. B) the main surface, no porosity can be observed, but a net like structure on a view corners, which is highly porous.....	47
Figure 28 SEM picture investigating in the pore size of AC, activated at 800°C.....	48
Figure 29 IR data exhibiting the decrease of functional groups during the activation process, depending on temperature.....	49
Figure 30 Fabrication of the electrode (10 mm) by stamping the doctor bladed, activated cellulose on the aluminum carrier.....	51
Figure 31 Evolution of the cell potential versus time during galvanostatic cycling at varying rates as indicated in the graph. Rates are absolute currents.	54
Figure 32 Galvanostatic cycling of symmetric SCs between 0 and 2.3 V at 1.5, 3, 9, 18, 36, 75 and 18 mA for 5 cycles each. The left column shows the specific capacitance and the right column the coulombic efficiency. The electrode material activated at 800°C (a) exhibits higher capacities due to smaller pore sizes. (b) has a similar composition but the carbon was activated at 950°C. The influence of conductive carbon content was investigated in (c). It contained 10% of conductive carbon, leading to more capacity fading as also reflected in lower initial efficiencies. All results were compared to (d) using an established electrode material, namely PICA (Jacoby Carbon Company).	55
Figure 33 Single CV cycle for an electrode material activated at 800°C containing about 15% binder recorded at a scan rate of 2 mV/s between 0 and 2.3 V.....	56
Figure 34 Testing electrode material activated at 800°C containing about 15% binder with organic electrolyte over 36 cycles, plotting specific capacitance calculated out of CV data in dependency of the voltage.....	57
Figure 35 Leak current diagram, after two hours the electrodes activated at 800°C containing 15% binder reached the plateau of a constant current.....	58
Figure 36 The self discharge diagram of electrodes manufactured like MH6 (Activated at 800°C; 15% binder) The supercapacitor needed 325.5 minutes to be semi-charged.....	59
Figure 37 Galvanostatic measurements with aqueous electrolytes, comparing capacities and coulombic efficiency for activated carbons (800°C) containing about 15% binder. Comparing the electrolytes (a) 1 M H ₂ SO ₄ with (b) 6 M KOH.	60
Figure 38 Galvanostatic measurements of the MH6 electrodes with KOH as electrolyte. Plotting the specific capacitance compared to the voltage.....	61
Figure 39 Images of electrodes after electrochemical characterization. (a) is with an alkaline as electrolyte (KOH), whereas (b) is measured with H ₂ SO ₄	62
Figure 40 The electrode material was activated at 800°C containing 15% binder. Comparing galvanostatic charge/discharge cycles for organic and aqueous electrolytes. a) TEABF ₄ /ACN as electrolyte showed highly reproduceable cycles. (b) used 6 M KOH as electrolyte losing consequently energy between charge and discharge, 1 M H ₂ SO ₄ was assembled in (c), a high amount of energy is put into the system without any reasonable output.....	63
Figure 41 Comparing CV data of supercapacitors using KOH and TEABF ₄ /ACN as electrolyte (Electrodes containing AC activated at 800°C with 15% binder).	63

8.2. Tables

Table 1 Comparing constituents of main wood species ¹	2
Table 2 Comparison between mechanical and chemical fines ¹⁰	7
Table 3 Structural property differences between mechanical and chemical pulp. ³	9
Table 4 Comparing fiber specific properties between mechanical and chemical pulp	10
Table 5 Comparing different activation types for fines.....	34
Table 6 Composites of fines with CNCs to increasing the surface area proved via BET.	36
Table 7 Composition of different electrode slurries	37
Table 8 Cyclic voltammetry settings for testing supercapacitors.	39
Table 9 Galvanostatic settings for testing supercapacitors.	39
Table 10 All chemicals applied in experiments	41
Table 11 ICPMS analysis, of sodium and sulfur content in fines.....	43
Table 12 BET analysis comparing the differences of the surface area of various activation processes.	43
Table 13 Comparing surface area of activated primary and secondary fines, measured through BET measurements.....	44
Table 14 BET analyzing the differences of the surface area of polymer-coated fines.....	45
Table 15 Determination of the surface area of mixed wooden composites.....	46
Table 16 Trace analysis by EDX to determine impurities in activated carbons.....	49
Table 17 Impedance data of the activated carbon electrodes, varying slurry compositions.	52
Table 18 Impedance results for PANi tablets, measured by EIS.	52
Table 19 Impedance results for PPy tablets, measured by EIS.	53

8.3. Bibliography

1. Fengel, D. & Grosser, D. Chemical composition of softwoods and hardwoods---A bibliographical review. *Holz als Roh- und Werkst.* **33**, 32–34 (1975).
2. Lönnberg, B. & Yhdistys, S. P.-I. *Mechanical Pulping*. (Fapet Oy, 2005).
3. Niskanen, K. *Paper Physics*. (Paperi ja Puu Oy, 2008).
4. Retulainen, E. *et al.* Papermaking Quality of Fines from Different Pulps - the Effect of Size, Shape and Chemical Composition. *Appita J.* **55**, 457–460 (2001).
5. Kang, T. & Paulapuro, H. Characterization of chemical pulp fines. *TAPPI J.* **5**, 25–28 (2006).
6. Gruber, H. M. Evaluation of fines content in pulps and filtrates in pulp production lines. (TU Graz, 2014).
7. Lindström, T. & Glad-Nordmark, G. Chemical characterization of the fines fraction from unbleached kraft pulps . *Svensk Papperstidning* 489–492 (1978).
8. Lin, T., Yin, X., Retulainen, E. & Nazhad, M. M. Effect of Chemical Pulp Fines on Filler Retention and Paper Properties. *Appita* **60**, 469 (2007).
9. Asikainen, S., Fuhrmann, A., Ranua, M. & Robertsén, L. Effect of birch kraft pulp primary fines on bleaching and sheet properties. *BioResources* **5**, 2173–2183 (2010).
10. Krogerus, B. *et al.* *Fines in closed circuits - Final report*. KCL (2002).
11. Sundberg, A., Pranovich, A. & Holmbom, B. Chemical characterization of various types of mechanical pulp fines. *J. Pulp Pap. Sci.* **29**, 173–178 (2003).
12. Cole, C. A., Hubbe, M. A. & Heitmann, J. A. Water Release from Fractionated Stock Suspensions. 1. Effects of the Amounts and Types of Fiber Fines. *Tappi J.* **7**, 28–32 (2008).
13. Simon, P. & Gogotsi, Y. Materials for electrochemical capacitors. *Nat Mater* **7**, 845–854 (2008).
14. Von Helmholtz, H. Ueber einige Gesetze der Vertheilung elektrischer Ströme in körperlichen Leitern, mit Anwendung auf die thierisch-elektrischen Versuche. *Ann. Phys. (N. Y.)* 211–233 (1853).
15. Becker, H. I. Low voltage electrolytic capacitor. *US Patent 2 800*, 616 (1957).
16. Stern, O. The Theory of the Electrolytic Double-Layer. *Zeit Elektrochem* **30**, 508–516 (1924).
17. Simon, P., Gogotsi, Y. & Dunn, B. Where Do Batteries End and Supercapacitors Begin? *Science* **343**, 1210–1211 (2014).
18. Liew, S. Y., Thielemans, W. & Walsh, D. A. Polyaniline- and poly(ethylenedioxythiophene)-cellulose nanocomposite electrodes for supercapacitors. *J. Solid State Electrochem.* **18**, 3307–3315 (2014).
19. Wang, H. *et al.* Bacterial cellulose nanofiber-supported polyaniline nanocomposites with flake-shaped morphology as supercapacitor electrodes. *J. Phys. Chem. C* **116**, 13013–13019 (2012).
20. Xu, D., Xiao, X., Cai, J., Zhou, J. & Zhang, L. Highly rate and cycling stable electrode materials constructed from polyaniline / cellulose. *J. Mater. Chem. A* **3**, 16424–16429 (2015).

21. Carlsson, D. O. *et al.* Electroactive nanofibrillated cellulose aerogel composites with tunable structural and electrochemical properties. *J. Mater. Chem.* **22**, 19014–19024 (2012).
22. Liu, Y., Zhou, J., Tang, J. & Tang, W. Three-Dimensional, Chemically Bonded Polypyrrole/Bacterial Cellulose/Graphene Composites for High-Performance Supercapacitors. *Chem. Mater.* **27**, 7034–7041 (2015).
23. Frackowiak, E., Meller, M., Menzel, J., Gastol, D. & Fic, K. Redox-active electrolyte for supercapacitor application. *Faraday Discuss.* **172**, 179–198 (2014).
24. Sim, C. K., Majid, S. R. & Mahmood, N. Z. Electrochemical performance of activated carbon derived from treated food-waste. *Int. J. Electrochem. Sci.* **10**, 10157–10172 (2015).
25. Dobeles, G., Dizhbite, T., Gil, M. V., Volperts, A. & Centeno, T. A. Production of nanoporous carbons from wood processing wastes and their use in supercapacitors and CO₂ capture. *Biomass and Bioenergy* **46**, 145–154 (2012).
26. Ma, G. *et al.* Nitrogen-doped porous carbon derived from biomass waste for high-performance supercapacitor. *Bioresour. Technol.* **197**, 137–142 (2015).
27. Hongying, X. I. A. *et al.* Preparation of high specific surface area activated carbon from walnut shell with KOH activation by microwave. *J. Porous Mater.* **22**, 1–10 (1981).
28. Cao, Y. *et al.* Hierarchical porous activated carbon for supercapacitor derived from corn stalk core by potassium hydroxide activation. *Electrochim. Acta* **212**, 839–847 (2016).
29. Li, W. *et al.* Effect of the gradient constant temperature on the electrochemical capacitance of cotton stalk-based activated carbon. *J. Solid State Electrochem.* **20**, 2315–2321 (2016).
30. Jurewicz, K., Pietrzak, R., Nowicki, P. & Wachowska, H. Capacitance behaviour of brown coal based active carbon modified through chemical reaction with urea. *Electrochim. Acta* **53**, 5469–5475 (2008).
31. Wang, C. *et al.* Sustainable synthesis of phosphorus- and nitrogen-co-doped porous carbons with tunable surface properties for supercapacitors. *J. Power Sources* **239**, 81–88 (2013).
32. Zhu, D. *et al.* Nitrogen-containing carbon microspheres for supercapacitor electrodes. *Electrochim. Acta* **158**, 166–174 (2015).
33. Skotheim, T. A. & Reynolds, J. *Handbook of Conducting Polymers*. (CRC Press, 2007).
34. Sarac, A. S., Ates, M. & Kilic, B. Electrochemical impedance spectroscopic study of polyaniline on platinum, glassy carbon and carbon fiber microelectrodes. *Int. J. Electrochem. Sci.* **3**, 777–786 (2008).
35. Zheng, Z. G. *et al.* Layer-by-layer nanocoating of lignocellulose fibers for enhanced paper properties. *J. Nanosci. Nanotechnol.* **6**, 624–632 (2006).
36. Lota, K., Sierczynska, A. & Acznik, I. Effect of aqueous electrolytes on electrochemical capacitor capacitance. *Chemik* **67**, 1142–1145 (2013).
37. Zhong, C. *et al.* *Electrolytes for Electrochemical Supercapacitors*. (CRC Press, 2016).
38. Sun, G. *et al.* Capacitive matching of pore size and ion size in the negative and positive electrodes for supercapacitors. *Electrochim. Acta* **56**, 9248–9256 (2011).
39. Toulouse, D. & Drexel, A. J. Charge storage mechanism in nanoporous carbons and its consequence for electrical. *Philos. Trans. R. Soc. A* **368**, 3457–3467 (2010).

40. Chen, L. *et al.* Metal-like fluorine-doped β -FeOOH nanorods grown on carbon cloth for scalable high-performance supercapacitors. *Nano Energy* **11**, 119–128 (2015).
41. Wang, Y. *et al.* Mesoporous Transition Metal Oxides for Supercapacitors. *Nanomaterials* **5**, 1667–1689 (2015).
42. Azhagan, M. V. K., Vaishampayan, M. V & Shelke, M. V. Synthesis and electrochemistry of pseudocapacitive multilayer fullerenes and MnO₂ nanocomposites. *J. Mater. Chem. A* **2**, 2152–2159 (2014).
43. Fischer, W. J. *et al.* Imaging of the formerly bonded area of individual fibre to fibre joints with SEM and AFM. *Cellulose* **21**, 251–260 (2014).
44. Kurniawan, F. *et al.* Carbon microsphere from water hyacinth for supercapacitor electrode. *J. Taiwan Inst. Chem. Eng.* **47**, 197–201 (2015).
45. Deng, J. *et al.* Inspired by bread leavening: one-pot synthesis of hierarchically porous carbon for supercapacitors. *Green Chem.* **17**, 4053–4060 (2015).
46. Wei, L., Sevilla, M., Fuertes, A. B., Mokaya, R. & Yushin, G. Hydrothermal carbonization of abundant renewable natural organic chemicals for high-performance supercapacitor electrodes. *Adv. Energy Mater.* **1**, 356–361 (2011).
47. Song, Y., Li, Z., Guo, K. kun & Shao, T. Hierarchically Ordered Mesoporous Carbon/Graphene Composites as Supercapacitor Electrode Materials. *Nanoscale* **8**, 15671–15680 (2016).
48. Sun, F. *et al.* Porous carbon with a large surface area and an ultrahigh carbon purity via templating carbonization coupling with KOH activation as excellent supercapacitor electrode materials. *Appl. Surf. Sci.* **387**, 857–863 (2016).
49. Kargl, R. *et al.* Functional patterning of biopolymer thin films using enzymes and lithographic methods. *Adv. Funct. Mater.* **23**, 308–315 (2013).
50. Sun, G. *et al.* Capacitive matching of pore size and ion size in the negative and positive electrodes for supercapacitors. *Electrochim. Acta* **56**, 9248–9256 (2011).
51. Pollak, E. *et al.* The Dependence of the Electronic Conductivity of Carbon Molecular Sieve Electrodes on Their Charging States. *J. Phys. Chem. B* **110**, 7443–7448 (2006).
52. Mourad, E. *et al.* Biredox ionic liquids: electrochemical investigation and impact of ion size on electron transfer. *Electrochim. Acta* **206**, 513–523 (2016).
53. Xie, Q. *et al.* Sustainable Low-Cost Green Electrodes with High Volumetric Capacitance for Aqueous Symmetric Supercapacitors with High Energy Density. *ACS Sustain. Chem. Eng.* **4**, 1422–1430 (2016).
54. Barzegar, F. *et al.* Preparation and characterization of porous carbon from expanded graphite for high energy density supercapacitor in aqueous electrolyte. *J. Power Sources* **309**, 245–253 (2016).